Deliverable 16.9: Chemo-mechanical processes in safety structures

Work Package 16

This project has received funding from the European Union's Horizon 2020 research and innovation programme 2014-2018 under grant agreement N°847593.

http://www.ejp-eurad.eu/

Document information

Project Acronym	**EURAD**
Project Title	**European Joint Programme on Radioactive Waste Management**
Project Type	**European Joint Programme (EJP)**
EC grant agreement No.	**847593**
Project starting / end date	**1st June 2019 – 30 May 2024**
Work Package No.	**16**
Work Package Title	**Chemo-Mechanical AGIng of Cementitious materials**
Work Package Acronym	**MAGIC**
Deliverable No.	**16.9**
Deliverable Title	**Chemo-mechanical processes in safety structures**
Lead Beneficiary	**ANDRA-LMDC**
Contractual Delivery Date	**January 2024**
Actual Delivery Date	**May 2024**
Type	**PU**
Dissemination level	**H**
Authors	**Layla Ibrahim (LMDC), Sebastian Gonzalez (CSIC), Laurie Lacarriere (LMDC), Víctor Vilarrasa (CSIC), Asta Narkuniene (LEI), Povilas Poskas (LEI), Alain Sellier (LMDC)**

To be cited as:

Ibrahim L., Gonzales S., Lacarriere L., Vilarrasa V., Narkuniene A., Poskas P., Sellier A. (2024): Title. Final version as of 28.05.2024 of deliverable D16.9 of the HORIZON 2020 project EURAD. EC Grant agreement no: 847593.

Disclaimer

Acknowledgement

This document is a deliverable of the European Joint Programme on Radioactive Waste Management (EURAD). EURAD has received funding from the European Union's Horizon 2020 research and innovation programme under grant agreement No 847593.

Status of deliverable		
	By	Date
Delivered (Lead Beneficiary)	Alain Sellier (ANDRA-LMDC)	01/12/2023
Verified (Task Leader)	ANDRA- LMDC	07/02/2024
Verified (WP leaders)	Alexandre Dauzères (IRSN)	19/02/2024
Reviewed (Reviewers)	Philippe Turcry LaSIE	15/05/2024
Approved (PMO)	Bernd Grambow	28/05/2024
Submitted to EC (Coordinator)	Andra (Coordinator)	30/05/2024

Executive Summary

The objectives of this deliverable are, first, to explain the scientific bases of the chemo-mechanical models used in the EURAD MAGIC 4.3 subtask in order to calculate the base case defined in the project. Next, the aim is to give results of chemo-mechanical simulations of base case study performed with the chemical models coupled with mechanical ones. For the three teams involved in this project, LMDC, LEI and CSIC, two types of information were expected, on the one hand the description of the chemical and mechanical modules of the chemo-mechanical models, on the other hand the application to the base case study provided by organizers. In this second part, the mesh and the boundary conditions are described first, then the chemical results and the mechanical esults of the simulations are discussed. The LMDC proposes a chemical model directly applicable at a structural scale, this model is derived from classical reactive transport models retaining only the most significant state variables. It provides the volumes of the hydrates and uses them in a mechanical homogenization module to calculate the elastic moduli of degraded concrete. These inputs are then used in a nonlinear model to compute the long-term behaviour of an underground structure (tunnel) until one million years. The CSIC model, based on a coupling between two existing simulation tools, remains at the scale of the host-rock/concrete interaction zone concerning the chemical part, which limits its use to the edges of the concrete structure. On the other hand, it integrates a simplification in terms of coupling with mechanics, which allows it to gain in efficiency on this second plan. LEI modelled coupled hydro-mechanical (HM) processes in parallel with reactive transport of solutes in concrete and rock porewater in two-dimensional space considering concrete liner and surrounding excavation disturbed zone.

Finally, the modelling strategy adopted by these three teams can be compared: LEI and CSIC adopted complete reactive transport models to describe the chemical processes close to the concrete/geological medium interface, while LMDC decided to develop a reduced reactive transport model retaining only transfer of main chemical species (calcium, carbon dioxide and water), but retaining all the other species as static reactive species. For CSIC and LEI, the strategy was to couple two softwares. The chemical analysis performed by CSIC could only be carried out until 25 years of aging due to the heavy computational cost of the coupling between the two softwares, and 10 000 years for LEI. The integration of all phenomena into a single software allowed to reach one million years for LMDC. Logically, the more sophisticated the coupling, the less the simulated duration. Concerning mechanics, LEI and CSIC used linear models with elastic parameters depending empirically to the chemical results. LMDC used a homogenization technic based on task 4.1 and task 3 results, to compute the elastic properties from the chemical results. LEI models the complete geometry, in 2D, proposed for the base case, considering the host rock as poro-elastic. LMDC considers the concrete in 3D and the host rock indirectly by its mechanical and chemical effects on the extrados of the tunnel. CSIC consider a few centimeters of concrete and host rock from either side of their interface. The limitation by CSIC of the size of the simulated area was still due to the excessively high calculation cost induced by the coupling between the two software programs. For LEI, the linearity of the mechanical behaviour laws allowed to consider the full geometry, but the computational cost limits the simulation to 10000 years. For LMDC, a model reduction of the concrete chemistry and of the hard rock mechanics allows to limit the size of the mesh and the number of main state variables, allowing to use a non-linear law for concrete until one million years. The non-linearity of the LMDC model considers the strain creep of the chemically degraded concrete, leading to a non-asymptotic radial displacement of the tunnel versus time under the host rock pressure, this, over one million years. Among these three modelling, the most complete in terms of chemistry was certainly the CSIC one, but the strategy to couple two softwares was penalizing regarding the computational cost, leading to reach only 25 years of aging for a small area of the tunnel close to its interface with the host rock. The LMDC strategy was less complete in terms of chemistry, but the proposed simplification of the chemistry and of the host rock allowed to predict the chemical evolution of concrete until the time of million years asked for the base case study. The LEI model was relatively complete in terms of chemistry, but linear in terms of mechanics, it allows to consider the full geometry in 2D, and the simulation reached a duration of 10 000 years.

Table of content

List of figures

List of Tables

1. Description of for the reactive transport models used at the structure scale

1.1 Reactive transport model of Andra-LMDC

To be applicable at structural scale, the LMDC model was formulated using a technic of "model reduction" allowing to limit the number of state variable in order to accelerate the computation. This technic takes advantage of chemical particularities of the problem to be studied to retain only the most explicative state variables. As explained below, considering the specificity of the Base Case, it was possible to summarize the chemistry of the concrete using only four variables (Calcium in solution, carbon dioxide, temperature and water saturation of the porosity). These four main state variables are solved directly on the mesh of a concrete tunnel in the framework of a finite element method. Despite the low number of principal state variables, this model is able to manage a greater number of accompanying state variables such as the amount of each hydrate in the cement paste, the mole number of calcite and the porosity of the concrete. The model considers also the dependence of transport coefficients to all these variables. Once clarified and implemented, this reactive transport model was coupled with a micro-mechanical model worked out in sub task 4.1 and 4.2, themselves based on micro mechanical model clarified in task 3, in relation with experimental results of task 2. The micro-mechanics model supplies the data for the macro mechanical model which, at this last scale considers non-linearity of the behaviour law, specifically the long-term creep of concrete.

Inputs of the model	**States variables**
Cement mineralogy	T: Temperature [K]
W/C	$[Ca^{2+}]$: Calcium in solution $\left[\frac{mol}{m^3}\right]$
Initial Saturation (Sr0)	$[CO_{2(aq)}]$: Total dissolved CO2 in water $\left[\frac{mol}{m^3}\right]$
Initial Temperature (T0)	$[W_L]$: Amount of water $\left[\frac{m^3}{m^3}\right]$

Figure 1.0: States variables and inputs of the Thermo-Hydro-Chemical model

1.1.1 The LMDC THCM reduced model

In order to predict the mechanical behaviour of the underground structure for radioactive waste disposal considering the chemical degradation, thermal and hydric condition, a reactive transport model is proposed to describe the degradation of the cement paste at structural scale. In order to be used at this scale, the chemical part of the model involves specific simplifications leading to a reduced model usable at macro scale. This thermo-hydro chemical model was developed on the basis of all the ionic species in porous solution and the variables in the different phases. The solid phases of cement hydrates, calcite precipitation and the physical properties of concrete (porosity and level of water saturation) are combined as internal variables in the model. The variables of this model are represented in the column $\overline{X}$ of Figure 1.1, X_i is the state variable for quantity . This model uses the cement mineralogy as initial condition. The balance equation (1) consider the chemical species and the thermal energy.

$$C_i \frac{\partial X_i}{\partial t} + div\left[-D_i(\overline{X}, \overline{V}_{(X)}).\overrightarrow{grad}\, X_i\right] = S_{X_i}(\overline{X}) - X_i \frac{\partial C_i}{\partial t} \quad (1)$$

Where C_i : capacity of variable X_i, $D_i(\overline{X}, \overline{V}_{(X)})$: diffusion coefficient , $S_{X_i}(\overline{X})$: source term.

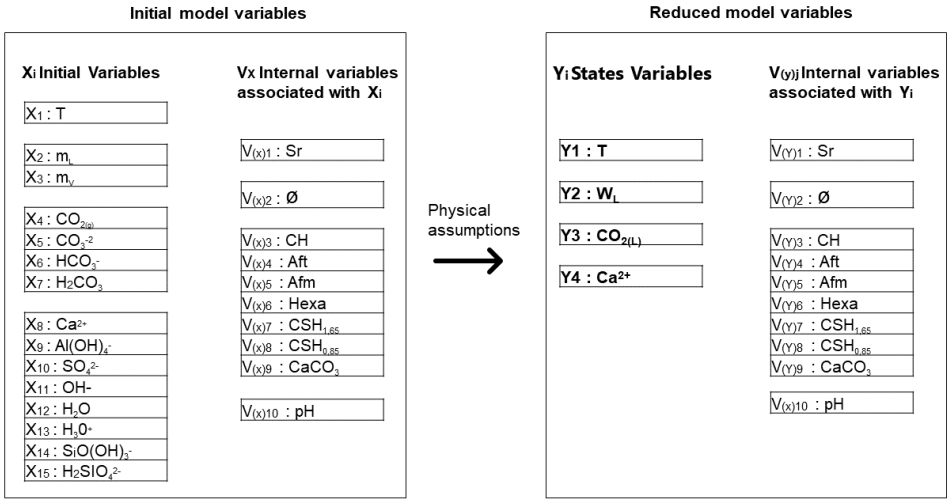

Figure 1.1: Variables of the Thermo-Hydro-Chemical model

There were two main assumptions to reduce the number of variables. The first is the instantaneous equilibrium between aqueous and solid phases, and the second is that, since calcium is the main component of the cement matrix, the equilibrium between hydrates depends mainly, as already proposed in [1] on calcium leaching. Thus, calcium in solution was chosen as one of the main state variables. As the boundary conditions of base case involve carbon dioxide, the carbonation of concrete must be considered, and consequently the carbon dioxide in solution is a main state variable. This selection allows the model to predict carbonation in a saturated environment. Nevertheless, as the base case tunnel model has a boundary condition of drying during the first 100 years of operation the drying and the re-saturation of the concrete must be modelled. In order to do that, water transport in concrete is described in a simplified manner in this model, where the state variable is limited to the water content. To describe the effect of temperature, one needed to consider the peak of temperature induced by the nuclear waste loading in the disposal, which is represented by a classical heat balance equation, where the temperature is the main state variable. The four main state variables chosen constitute the vector Y in Figure 1.1.

$$C_{eq}\frac{\partial \boldsymbol{Y_K}}{\partial t} + div\left[-D_{eq}(\overline{Y},\overline{V}_{(Y)}).\overrightarrow{grad}\,\boldsymbol{Y_K}\right] = S_{eq}(\overline{Y},\overline{V}_{(Y)}) \quad (2)$$

C_{eq} the equivalent capacity of species Y_K, $D_{eq}(\overline{X})$ the equivalent diffusion term, and $S_{eq}(\overline{X})$ the source term.

1.1.1.1 Balance equations

The governing equations of the thermo-hydro-chemical model for predicting the concrete behaviour are explained in details in this section.

- Mass conservation of carbon dioxide in solution

The carbon dioxide mass balance equation (3) is obtained by combining the mass balance equations of carbon dioxide in both gaseous and dissolved in water, and according to Henry law's to consider the solubility of carbon dioxide in water.

$$\begin{aligned}[\emptyset.S_L + K_H(T)\emptyset(1-S_L)]\frac{\partial \boldsymbol{CO_{2L}}}{\partial t} \\ + div\left[-(D_{CO_{2L}}(\overline{Y},\overline{V}_{(Y)}) + K_H(T).D_{CO_{2g}}(\overline{Y},\overline{V}_{(Y)})).\overrightarrow{grad}\,\boldsymbol{CO_{2L}}\right] \\ = S_{CaCO3\rightarrow CO_{2_L}} - \boldsymbol{CO_{2L}}\left(\frac{\partial \emptyset.S_L}{\partial t} + K_H(T).\frac{\partial \emptyset.S_L}{\partial t}\right)\end{aligned} \quad (3)$$

Where ∅: porosity, S_L: the degree of water saturation of pores, $D_{CO_{2L}}(\overline{Y},\overline{V}_{(Y)})$ and $D_{CO_{2g}}(\overline{Y},\overline{V}_{(Y)})$ are the diffusion coefficient respectively of aqueous and gaseous carbon dioxide $[m^2.s]$. $S_{CaCO3\rightarrow CO_{2L}}$ corresponds to the source term of dissolved carbon dioxide consumed by the calcite precipitation $[mol/m^3.s]$. The carbonate issued for dissolvec carbon dioxide reacts with the dissolved calcium in pore solution to form the calcite according to the following equation:

$$Ca^{2+} + CO_3^{2-} \rightarrow CaCO_3 \tag{4}$$

The carbonation reaction occurs with CO_3^{2-}. The concentration of CO_3^{2-} in solution depends on the pH of the medium. The pH of the medium is determined through the combination of electric balance, water dissociation, and the computation of ion concentrations.To take into consideration this effect, a function of pH is included into the source term (5) of equation (3) to describe the amount of dissolved carbon dioxide that can react to form calcite:

$$S_{CaCO3\rightarrow CO_{2L}} = -\emptyset.S_L.[Ca^{2+}].[CO_3^{2-}].Kc(T) = -\emptyset.S_L.[Ca^{2+}].\left[CO_{2(aq)}\right].f(pH).Kc(T) \tag{5}$$

The pH function $f(pH)$ prevents the calculation of calcite precipitation in low pH conditions. This function allows to reproduce the inibation of the precipitation of calcite in the underground rock (or soil) in contact with the concrete (pH in the rock is lower than in concrete and at these low pH the dissolved carbon is present in HCO3- form that leads to calcite precipitation. This function is presented in Figure 1.2, giving the proportion of CO_3^{2-} dissolved into the solution relative to the total dissolved carbon.

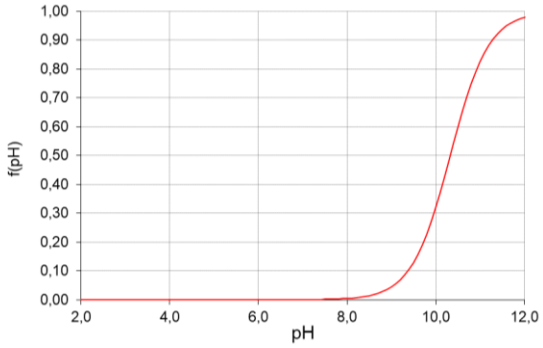

Figure 1.2 : pH function, representing the proportion of CO_3^{2-} as a function of pH

$Kc(T)$ describes the calcite kinetics of precipitation, depending on the temperature, it is expressed as a function of temperature using the Arrhenius law (6):

$$K_C(T) = K_0.exp\left(\frac{-E_A}{RT}\right) \tag{6}$$

- Mass conservation of calcium in solution

The mass balance of calcium in solution is written as follow (7):

$$\left(\emptyset.S_L + \frac{\partial Cas}{\partial Ca^{2+}}\right)\frac{\partial \boldsymbol{Ca^{2+}}}{\partial t} + div\left[-D_{Ca^{2+}}(\overline{Y},\overline{V}_{(Y)}).\overrightarrow{grad}\,\boldsymbol{Ca^{2+}}\right] = S_{CaCO3\rightarrow Ca^{2+}} - \boldsymbol{Ca^{2+}}.\frac{\partial \emptyset.S_L}{\partial t} \tag{7}$$

In this equation, the term $\frac{\partial Cas}{\partial Ca^{2+}}$ considers the progressive dissolution of cement hydrate when the calcium concentration in solution decreases. This term directly involves the effect of temperature on the equilibrium of hydrates. It is a function of the mineralogy of the cement paste, considering the amount

of each type of hydrate (portlandite, hexahydrates, ettringite, calcium silicate hydrates…). The detailed description of this term, as well as of the other coefficients of this balance equation, are described in the section below dedicated to the evolution laws. $D_{Ca^{2+}}(\overline{Y}, \overline{V}_{(Y)})$ is the diffusion coefficient.

- Mass balance of water

The water transport at macroscopic scale is described by the balance equation of water content $\boldsymbol{W_L}$ (8) [2]:

$$\frac{\partial \boldsymbol{W_L}}{\partial t} + div\left[-D_{W_L}(\overline{Y}, \overline{V}_{(Y)}).\overrightarrow{grad}\,\boldsymbol{W_L}\right] = S_{WbL}(\overline{Y}, \overline{V}_{(Y)}) \quad (8)$$

In equation (8), $D_{W_L}(\overline{Y}, \overline{V}_{(Y)})$ is the transfert coefficient of water, the water source term S_{Wb} in the equation (9) describes the amount of water released by the dissolution of hydrates. It is expressed as follows:

$$S_{Wb} = V_{m_{H_2O}} \frac{\partial H_2O}{\partial Cas}.\frac{\partial Cas}{\partial Ca^{2+}}.\frac{\partial Ca^{2+}}{\partial t} \quad (9)$$

Where $V_{m_{H_2O}}$ is the molar volume of water, H_2O quantity of water released from hydrates dissolution.

- Heat balance equation

The evolution of temperature in the concrete is described by the following heat conservation equation:

$$\rho_c.\mathrm{C}_c \frac{\partial \boldsymbol{T}}{\partial t} + div\left[-\lambda_c.\overrightarrow{grad}\,\boldsymbol{T}\right] = 0 \quad (10)$$

Where ρ_c : Concrete density, C_c specific heat capacity of concrete, λ_c concrete heat conductivity. These parameters are assumed constant in this model.

1.1.1.2 Evolution laws

Evolution laws link the main state variables (Ca, CO_2, W_L, T) with secondary state variables (portlandite, CSH…) in one hand, and secondary state variables with coefficients of balance equation (capacity, diffusion or source terms). They are the main causes of non-linearity of the model, they allow to consider all the coupling between state variables of the chemical module of the global model.

- Thermodynamic equilibrium curve

The modelling of the calcium leaching is based on the thermodynamic equilibrium curves which describe the progressive dissolution of the hydrates in the cement matrix as a function of calcium concentration in the poral solution. These curves also consider the effect of the temperature on the thermodynamic equilibrium through a shift of calcium concentration at the equilibrium versus the temperature. For example, the dissolution reaction of portlandite is written as follow:

$$Ca(OH)_2 \rightarrow Ca^{2+} + 2OH^- \quad (11)$$

The equilibrium concentration of calcium for the dissolution of portlandite is obtained by a thermodynamic equilibrium, for instance at 25°C:

$$[Ca^{2+}][OH^-]^2 = 10^{-pK(25°C)} \quad (12)$$

The dissolution reactions and thermodynamic equilibrium data used to calculate equilibrium calcium concentrations for all hydrates are taken from reference [3].

To shift this equilibrium concentration as a function of temperature, an exponential law (13) is calibrated:

$$Ca^{2+}_{eq(T)} = Ca^{2+}_{eq(T0)} exp\left[-\frac{E_A}{R}\left(\frac{1}{T}-\frac{1}{T_0}\right)\right] \quad (13)$$

where $E_A\ (J/mol)$ is a constant to be determined for each hydrate.

The calcium leaching consists in a progressive dissolution of the cement matrix. For that reason, an elementary dissolution function is used (14):

$$f_{V_{(Y)j}}(Ca^{2+}) = 1 - exp\left[\frac{-1}{m_j}\left(\frac{[Ca^{2+}]}{\left(\frac{1}{m_j.\ln(2)}\right)^{1/m_j}.\left[Ca^{2+}_{eq(T)}\right]_{V_{(Y)j}}}\right)^{m_j}\right] \quad (14)$$

where $[Ca^{2+}]$ is the concentration of calcium in solution , $\left[Ca^{2+}_{eq(T)}\right]_{V_{(Y)j}}$ is the equilibrium concentration of calcium in solution for each hydrate $V_{(Y)j}\ (j = 3 \dots 8)$, m_j is a parameter to fit for each hydrate based on the thermodynamic data base [16].

This function varying between 1 (initial state of hydrate) and 0 (totally leached cement paste) describes the progressive dissolution of each hydrate. It is derivable and gives the proportion of remaining hydrate as a function of the concentration of calcium in the interstitial solution. Moreover, this function is smoothed, which avoids the sudden dissolution of hydrates and then the corresponding problems of converge of the finite element method.

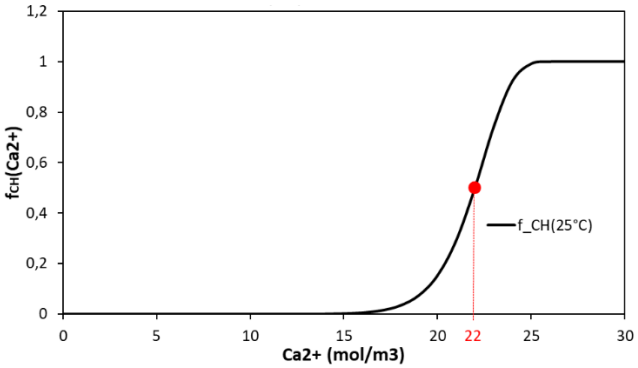

Figure 1.3: Thermodynamic equilibrium curve of Portlandite at 25°C

In order to obtain the variation of bound calcium in solid, the function (14) is multiplied by the maximum amount of solid calcium in each hydrate, which usually corresponds to the state of the cement matrix at the end of the hydration process (according to the hypothesis of a full hydration).

$$Cas_{V_{(Y)j}}(Ca^{2+}) = f_{V_{(Y)j}}(Ca^{2+}) \times Cas\_max_{V_{(Y)j}} \quad (15)$$

The equilibrium calcium concentrations are calculated for each of the hydrates of the cement paste, and the initial quantity of hydrates is calculated by solving a system equation according to the cement mineralogy [4]. Thus, the composition of the cement is considered, and the total equilibrium curve is obtained by adding the elementary curves of each hydrate. Figure 1.4 represents the total equilibrium curve for CEMI at the temperature of 25°C, and Figure 1.5 represents the equilibrium curve of CEMV at 25°C. These two figures illustrate the capability of the model to consider different types of cement despite its low number of main state variables. The curves show specifically the particular initial mineralogy of CEMV based concrete characterised by the lack of portlandite.

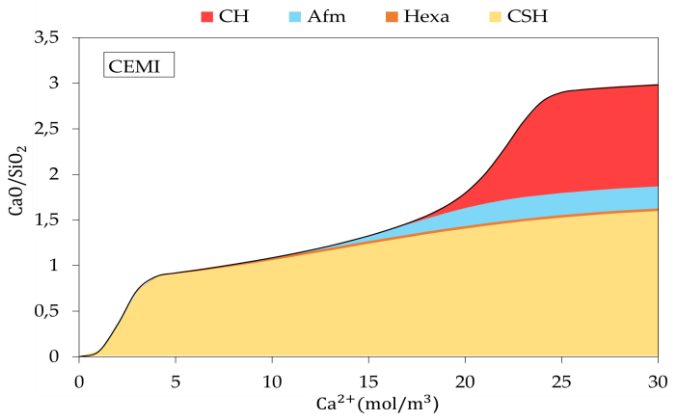

Figure 1.4 : Equilibrium curve of CEMI at 25°C

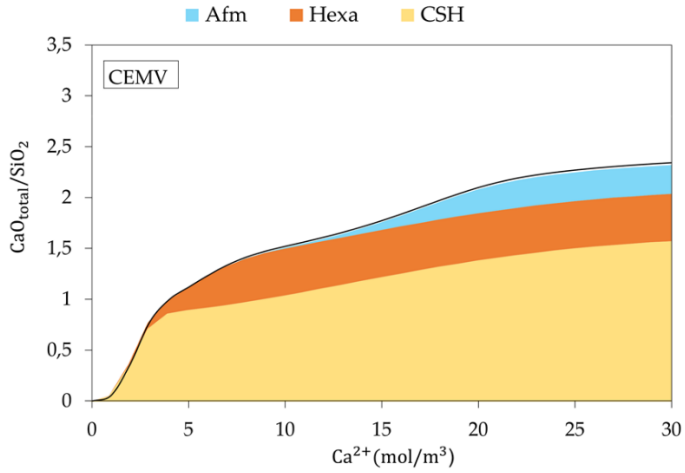

Figure 1.5: Equilibrium curve of CEMV at 25°C

The amount of water released by hydrate dissolution is calculated in the same manner, using the elementary functions of hydrates dissolution and multiplying by the total amount of water in each hydrate ($H_2O\_max_{V_{(Y)j}}$ in equation 16):

$$H_2O_{V_{(Y)j}}(Ca^{2+}) = f_{V_{(Y)j}}(Ca^{2+}) \times H_2O\_max_{V_{(Y)j}} \quad (16)$$

Thus, the source term of equation (9) comes as follows from the quantity of water released by hydrate dissolution:

$$\boldsymbol{S_{W_b}} = V_{m_{H_2O}} \sum_{V_{(Y)j}} H_2O\_max_{V_{(Y)j}} . \frac{\partial f_{V_{(Y)j}}(Ca^{2+})}{\partial Ca^{2+}} . \frac{\partial Ca^{2+}}{\partial t} \quad (17)$$

- Porosity

A porosity model takes into account hydrate dissolution and calcite precipitation as follows:

$$\emptyset_{(t)} = \emptyset_0 + V_{H(t)} - V_{C(t)} \quad (18)$$

Where $\emptyset_0$: the initial porosity of concrete, $V_{H(t)}$: current volume fraction of hydrates, and $V_{C(t)}$: current volume fraction of calcite.

- Diffusion coefficient

The diffusion coefficient is described as a function of porosity and degree of water saturation (19).

$$D_{e\,T_0(Yi)}(\emptyset, S_L) = f(S_L, \emptyset).D_{T_0(Yi)} \tag{19}$$

The diffusion coefficient of Ca^{2+}, $CO_{2(g)}$ and $CO_{2(L)}$ are directly taken from the literature [5][6][7] and [8]. For water transport, the water transfert coefficient depends on the remaining water volume in the material, as described by the law proposed by Mensi [2] (Details summarised in Table 1).

The effect of temperature on diffusion coefficients is described by an Arrhenius law's (21) with E_A being the activation energy:

$$D_e(T) = D_e(T_0).exp\left(\frac{-E_A}{R}\left(\frac{1}{T} - \frac{1}{T_0}\right)\right) \tag{20}$$

Table 1. Diffusion coefficients and other parameters used in the THC model

Species Yi	$f(\emptyset, S_L)$	$D_{T_0(Yi)}(\,m^2.s^{-1})$	$\frac{E_A}{R}\,(K)$	References
Ca^{2+}	$\frac{\exp(9{,}95\emptyset)}{(1+625(1-S_L)^4)}$	$2{,}3.10^{-13}$	8009,15	[5], [9]
$CO_{2(g)}$	$\emptyset^a.(1-S)^b$ a and b are fitted	$1{,}6.10^{-5}$	6258	[6], [7], [10]
$CO_{2(L)}$	$4.\frac{\emptyset.S^4}{\pi^2}$	$9{,}55.10^{-10}$	4269,9	[8], [11], [12]
W_L	$\exp\,(50.\emptyset.S_L)$	8.10^{-13}	4600	[2], [13]

1.1.1.3 Numerical implementation

The equations (3)(7)(8) and (10) of the THC model have been implemented in the finite element code Cast3M developed at CEA. The inputs of the model are: cement mineralogy (seeTable 2); initial relative humidity; water to cement ratio; temperature and the partial pressure of carbon dioxide.

Table 2. Amount of cement hydrates (issued from hydration model [14]

Amount of Hydrates (mol/ m3 of cement paste)	
CH	4501.12
Aft	0
Afm	292.23
Hexa	23.3
CSH	3570.24

The model equations are solved using an iterative approach through the classical finite element method and an implicit scheme for time and space. At the beginning of the time step, the capacity and diffusion term attributed to the material are initialized and also the source term of the conservation equation. Once

the initial state is identified, the resolution of the equations starts in the convergence loop where, at each iteration, the capacity, diffusion and source terms are updated until the convergence criterion is verified. The outputs of the model are: the remaining quantity of each hydrate in the cement paste, the degree of saturation in water and the porosity. These results are the input of the mechanical model described in chapter 2. An overview of the model resolution flow is showed in the Figure 1.6.

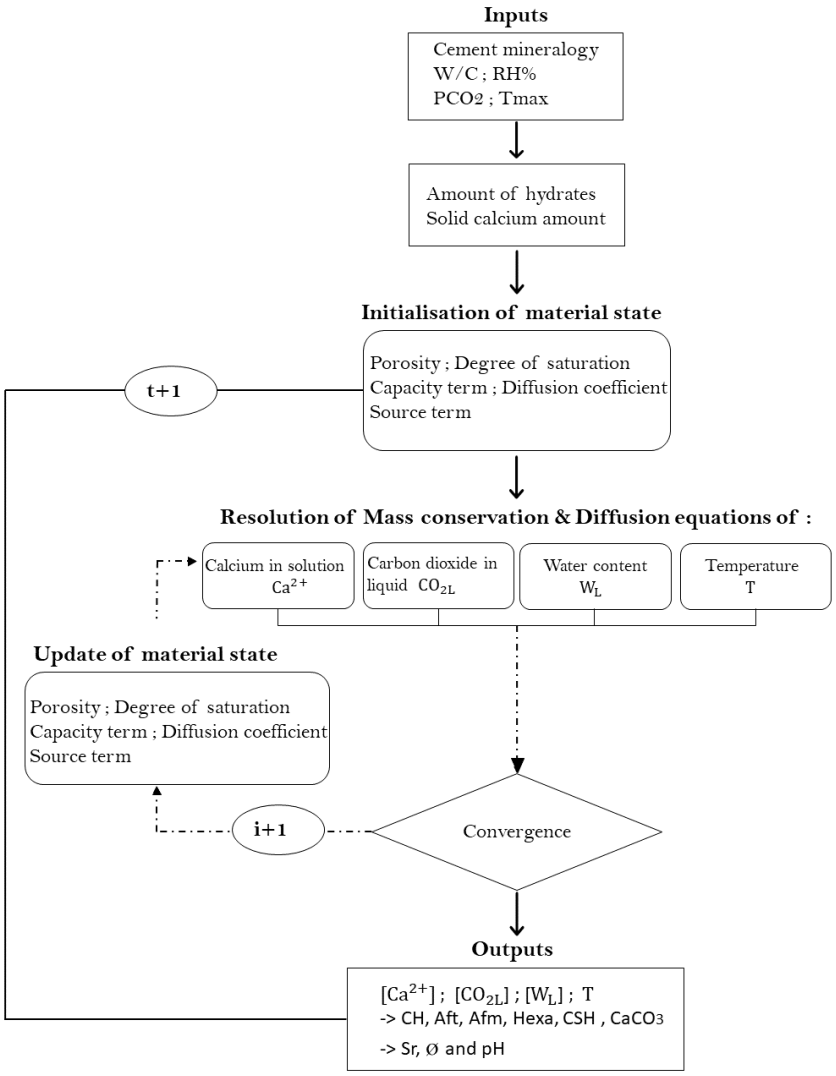

Figure 1.6: Algorithm of resolution of LMDC chemical module implemented in Castem software to compute the base case study (t : time, i : iteration allowing to control the convergence)

1.1.2 Calibration and Validation of the model

The chemical model was first tested on decalcification tests in saturated conditions and for different temperatures to ensure the proposed law are able to reproduce the dissolution of hydrates. Once validated, the model is confronted to carbonation tests in partially saturated conditions. The validation is based on the comparison between numerical results and experimental measurements.

1.1.2.1 Leaching of calcium

The calcium leaching test conducted by Peycelon [9] on CEM I cement paste samples have been modelled under saturated condition and different temperature (25°C, 50°C and 85°C). The specimens of hardened cement paste used were cylindrical 1.5 to 2 cm high and 7 cm in diameter, the leaching is a unidirectional degradation of the sample. Due to the symmetry, only the half-height of the sample is modelled. The mesh used in the simulation is fine enough to capture the variations in the solution

concentration and hydrates dissolution occurring near the surface of the specimen. The Dirichlet condition is used at the surface in contact with pure water to represent leaching boundary condition ($[Ca^{2+}] = 0\ mol/m^3$). The amount of calcium released have been measured experimentally and can be compared to the results of the numerical simulations at different temperatures. The model is able to reproduce the experimental results with a high degree of accuracy. The effect of temperature is well reproduced, the amount of leached calcium increases with temperature as illustrated in Figure 1.7.

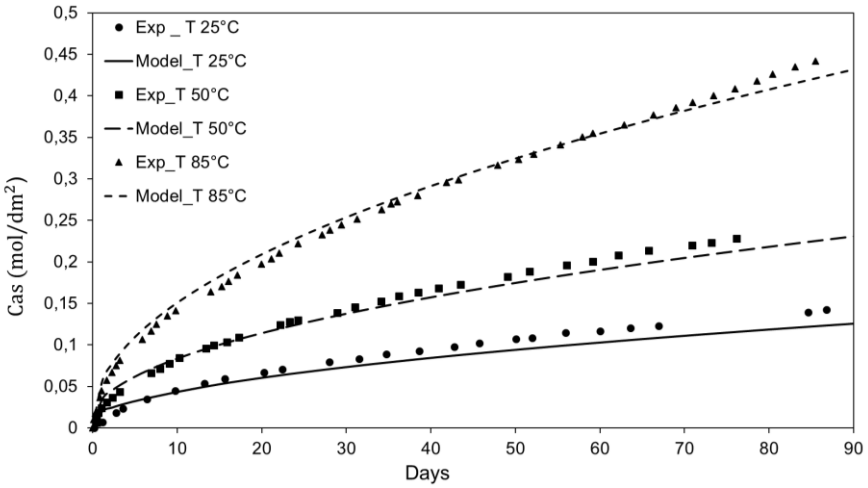

Figure 1.7 : Experimental results from Peycelon [9] compared to numerical results of cumulated released calcium as a function of time for different temperatures

The porosity profiles show the influence of calcium leaching on the microstructure (Figure 1.8). The increase of porosity is due to the dissolution of hydrates, specifically the dissolution of portlandite which creates more voids. These profiles illustrate the impact of chemical reactions on the overall porosity distribution within the material, highlighting areas where the dissolution process has significantly influenced on the microstructure.

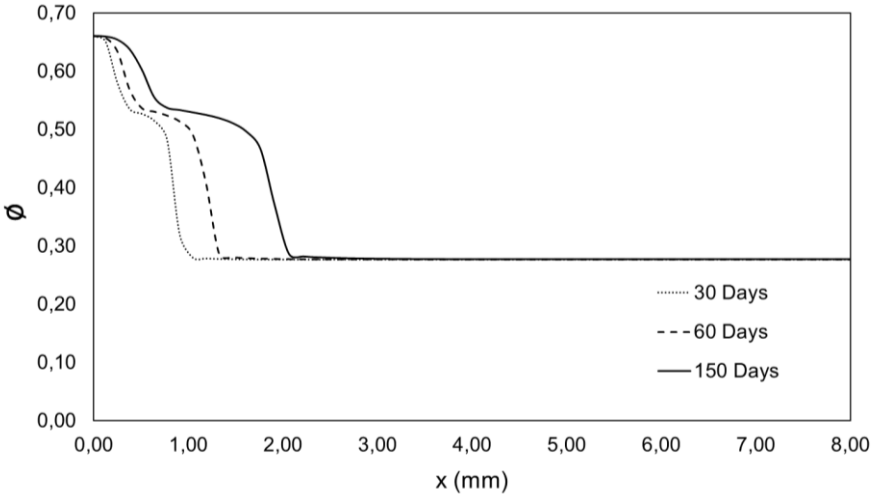

Figure 1.8: Simulated porosity profiles for different times at a temperature of 25°C for CEMI cement paste [9]

1.1.2.2 Carbonation test:

The carbonation test carried out by Hyvert [15] on mortar specimens of CEMI under unsaturated condition have been reproduced for two different partial pressures of carbon dioxide ($P_{CO2} = 0.03\%\ atm$ and $P_{CO2} = 10\%\ atm$). The cylindrical samples are modelled in 2D axisymmetric mode by using 4 node quadrilateral finite elements. The degradation of the samples was guaranteed to be unidirectional. The experimental tests were performed at a controlled temperature of 20 °C ± 0.5 °C and a relative humidity

of 65% ± 5% (uncarbonated specimens initially equilibrated to this RH and temperature). The boundaries conditions are defined at the surface in contact with the atmosphere in terms of concentration of carbon dioxide (0.03% or 10% of partial carbon dioxide pressure), and to maintain the relative humidity at the surface (RH = 65%). The numerical results simulation are shown in Figure 1.9 compared to the experimental results. Experimental points are shown with a difference between mean depth and extreme values of up to 3 mm [16], which could explain some differences between the numerical and experimental results. However, the model is able to reproduce the different behaviour of carbonation depending on the partial pressure of carbon dioxide.

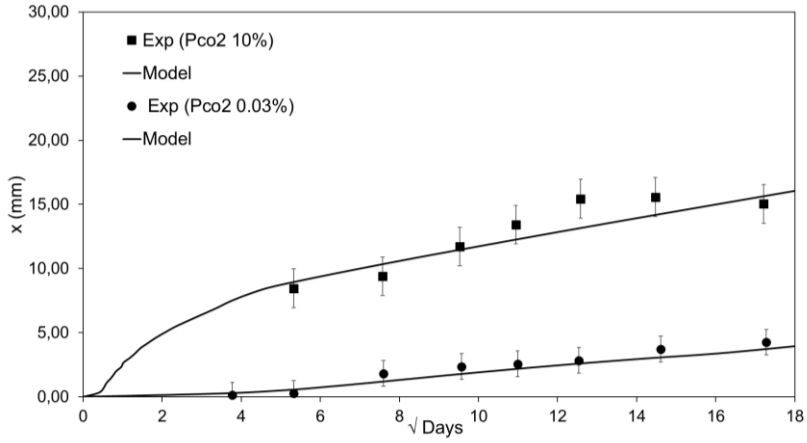

Figure 1.9 : Experimental results from Hyvert et al. [15] Carbonation depth (x) compared to numerical prediction for two partial pressures of carbon dioxide at the boundary condition

The model supplies the remaining quantity of hydrates after degradations as shown in Figure 1.10. This reaction leads to the dissolution of hydrates in the concrete matrix and their partial conversion in calcite.

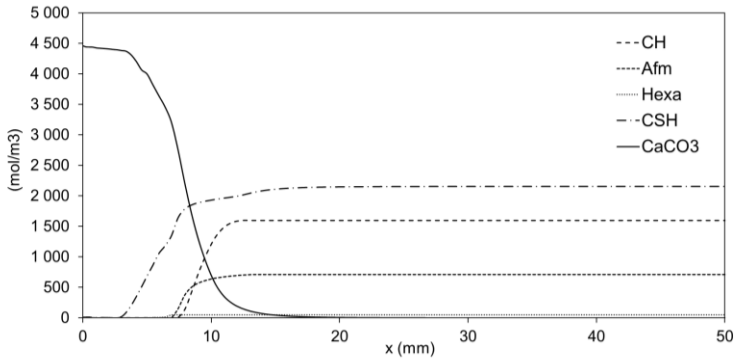

Figure 1.10 : Simulated profiles of solid phases after 1 year of carbonation at 10% CO_2 partial pressure

1.1.2.3 Summary of the LMDC chemical model of concrete

This THC model is based on four non-linear balance equations, which are solved using an implicit scheme. The chemical model considers the thermodynamic equilibrium of cement hydrates with the pore solution, taking into account the effect of temperature on this equilibrium and then on degradation. This model differentiates cement paste hydrates and manage calcite precipitation thanks to internal variables. Pore volume and water content are deduced from these internal variables. The mass balance equations were successfully implemented in the Cast3M finite element tool and validated against literature experimental data on calcium leaching and carbonation. The model is now able to predict parameters essential for chemo-mechanical calculus, such as porosity, profile saturation, remaining hydrates and amount of precipitated calcite.

1.1.3 Coupling with mechanical model:

In order to couple the thermo-hydro-chemical (THC) model described above with the mechanical model, it is necessary to determine the mechanicals properties of the concrete. Elastic constants are deduced from volumetric fractions of phases computed by the THC model, the method is based on the homogenisation technique. In this model, the cement paste undergoes two chemical degradations, the first one is the calcium leaching, which leads to dissolution of hydrates and a decrease in mechanical properties. On the other hand, the cement paste can be subjected to carbonation where a new solid phase, i.e., calcite, is formed, and then the porosity decreases and the mechanical properties are enhanced. The homogenization model takes into consideration these two antagonist effects. As shown in Figure 1.8 and Figure 1.10, the chemical model described above provides the phases volumes at each time step. These phases volumes are the data for the elastic homogenization of the cement paste. The Figure 1.11 represents the scheme of homogenisation, there is two level of homogenisation. The first one is to homogenize the cement paste based on the mineralogical state and the second level is to determine the elastic properties of the concrete considering the fraction volume of aggregates and sand.

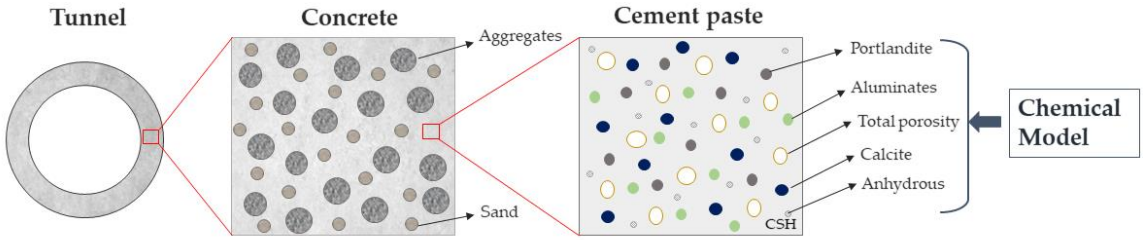

Figure 1.11 : Scheme of the multi-scale THCM model developed for the study of the durability of concrete tunnels for the Base Case.

The Mori-Tanaka scheme is applied [17] for the two levels.

$$\begin{cases} K_{hom} = \left(k_m + \frac{4}{3}\mu_m \sum_{i=1}^{n} c_i \frac{k_i - k_m}{k_i + \frac{4}{3}\mu_m}\right)\left(1 - \sum_{i=1}^{n} c_i \frac{k_i - k_m}{k_i + \frac{4}{3}\mu_m}\right)^{-1} \\ \mu_{hom} = \left(\mu_m + f_m \sum_{i=1}^{n} c_i \frac{\mu_i - \mu_m}{\mu_i + f_m}\right)\left(1 - \sum_{i=1}^{n} c_i \frac{\mu_i - \mu_m}{\mu_i + f_m}\right)^{-1} \end{cases} \quad (21)$$

$$f_m = \frac{\mu_m(9k_m + 8\mu_m)}{6(k_m + 2\mu_m)}$$

Where k_m and μ_m the properties of the matrix, k_i and μ_i for the inclusions and c_i the fraction.

The elastic compressibility and shear modulus of the cement paste (Kp_{hom}, μp_{hom}) are determined by equation (21). At this homogenization level, the matrix consists of the solid CSH defined by its property's km and μm [18]. This scheme considers the volumetric fractions of the inclusions, denoted as c_i, determined by the chemical model. Subsequently, the homogeneous properties of concrete are determined using the Mori-Tanaka scheme at a second level (Figure 1.11), where the matrix represents the cement paste homogenized at the first level, and the inclusions consist of sand and aggregates.

The validation of this homogenization scheme was performed through a comparison between the paste homogenization model and a microhardness test conducted by Danèse [19]. The Figure 1.12 represents the normalized elastic modus of the cement paste versus the main chemical state variable (calcium in solution).

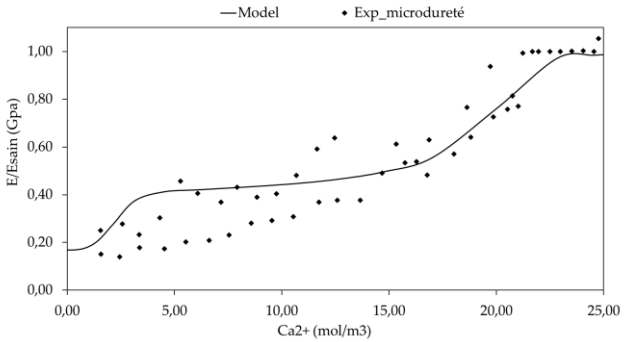

Figure 1.12 : Calculation of the Young's modulus of the paste as a function of the predicted calcium in solution using the Mori-Tanaka homogenization scheme, and comparison with the experimental data points from the microhardness test conducted by Danèse[19].

The poro-mechanical model coupled to the thermo-hydro-chemical model is performed in LMDC Toulouse. This model, called FLUENDO3D and implemented in the finite element code Cast3M, is now available online on CEA web site of Castem. This model combines a nonlinear visco-elastic module, a plastic module and a damage module for the concrete and a possibility to model reinforcements [20]. As the long-term behaviour of concrete is mainly controlled by creep, basic creep constitutive equations are used alongside a plastic strains model, ensuring compatibility of the stress field with the strength criteria. The basic creep model considers two typical rheologic modules: a Kelvin solid for reversible creep and a nonlinear Maxwell viscoelastic fluid for permanent creep, as shown in Figure 1.13. and detailed in [21]. In this model, the kinetics of the creep depends directly on the change of the elastic young modulus and Poisson ratio determined by homogenization equation (21). So, when the carbonation increases the Young modulus, the creep rate decreases, while it increases automatically in case of leaching as illustrated in [4].

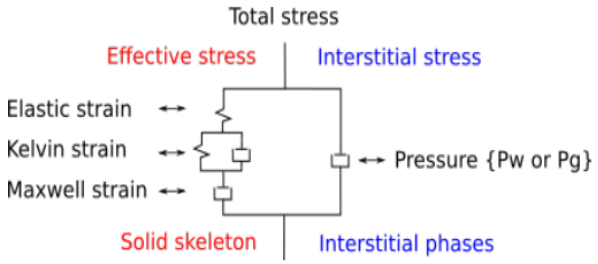

Figure 1.13 : Idealized rheologic scheme for poro-mechanics creep model, according to [21]

Some results of the calculus of tunnel proposed as base case are presented in chapter 2 of the present report.

1.2 Reactive transport model of LEI

LEI performed reactive transport simulations of concrete-host rock environment with numerical tool iCP. Modelling of solutes, CO_2 transport (in gaseous and aqueous form) and subsequent chemical interactions with concrete minerals allow to assess important processes such as minerals dissolution and precipitation, changes in porewater pH and dissolved species concentration. Subsequently, minerals' dissolution/precipitation induced changes in porosity could be assessed and provided feedback into transport simulation and mechanical deformation analysis.

1.2.1 iCP interface model

iCP is an interface developed by Amphos21 (Spain) to couple two standalone simulation programs: the general purpose Finite Element platform COMSOL Multiphysics and the geochemical code PHREEQC [22]. The main goal of the interface is to take advantages and capabilities of mentioned codes, providing

a numerical platform that can efficiently simulate a wide number of multiphysics problems coupled with geochemistry. iCP is written in Java and uses the IPhreeqcC++ dynamic library and the COMSOL Java-API. The geochemical reactions are solved in parallel by balancing the computational load over multiple threads.

Reactive transport modelling requires information on flow conditions which are governed by materials hydraulic properties (intrinsic and relative permeability, initial porosity, water retention curve), transport related properties (tortuosity, solute diffusivity in water, saturation), chemistry related data (equilibrium constants of chemical reactions considered in the analysis, activity coefficients) as well as pore water solution composition, amount of minerals in porous medium and initial and boundary conditions. Chemistry related data are provided in section 1.2.2, flow and mechanics related parameters are presented in section 2.2.

1.2.2 Thermodynamic data

For the analysis of the hydrated cement phase assemblage and pore water chemical composition, thermodynamic database Cemdata18 [23] was considered. The Cemdata18 database has been developed specifically for hydrated Portland, calcium aluminate, calcium sulfoaluminate and blended cements, as well as for alkali-activated materials. It is available in GEMS and PHREEQC computer program formats, and includes thermodynamic properties determined from various experimental data published in recent years. Cemdata18 contains thermodynamic data for common cement hydrates such as C-S-H, AFm and AFt phases, hydrogarnet, hydrotalcite, zeolites, and M-S-H that are valid over temperatures ranging from 0 to at least 100 °C. Solid solution models for AFm, AFt, C-S-H, and M-S-H are also included in the Cemdata18 database. CSHQ [24] model has been selected for cement hydration modelling in this study. Key data of this model is summarized in Table 3.

Table 3. Solid solution model of C-S-H (CSHQ solid solution) [23]

Phase	$\Delta_f G^0$	$\Delta_f H^0$	S^0	a^0	V^0
End member	(kJ/mol)	(kJ/mol)	(J/K/mol)	(J/K/mol)	(cm^3/mol)
TobH Ca/Si=0.67: $C_{2/3}SH_{1.5}$	-1668.56	-1841.5	89.9	141.6	55
TobD Ca/Si=1.25: $C_{5/6}S_{2/3}H_{1.83}$	1570.89	-1742.4	121.8	166.9	48
JenH Ca/Si=1.33: $C_{1.33}SH_{2.17}$	-2273.99	-2506.3	142.5	207.9	76
JenD Ca/Si=2.25: $C_{1.5}S_{0.67}H_{2.5}$	-2169.56	-2400.7	173.4	232.8	81
NaSH: $N_{0.5}S_{0.2}H_{0.45}$	-431.20	478.0	41.2	37.9	10.5
KSH: $K_{0.5}S_{0.2}H_{0.45}$	-440.80	-489.6	48.4	40.6	12.4

As indicated in [23], CSHQ model was developed in order to address some known shortcomings of the earlier CSH-I and CSH-II models namely insufficient connection to the C-S-H structure and the unrealistic assumption of ideal mixing between tobermorite-like and amorphous silica end members. In this Cemdata18 database, two end members for K and Na (similar to those from the ECSH model) were provisionally added to improve predictions of pH and composition of the Portland cement porewater.

For reactive transport modelling, the initial amount of minerals and porewater composition are required. Therefore, these input data were derived performing cement hydration simulation with PHREEQC and database Cemdata18. Following the cement composition provided in Table 2 [25], the cement hydration simulations were done assuming that limestone gravel and sand were inert materials.

Phase assemblage in hydrated cement was predicted with thermodynamic modelling of using oxide proportions, water to cement (w/c) ratio and curing temperature. The amount of oxides considered for CEM I hydration is summarized in Table 4.

Table 4. Cement CEM I chemical composition

Oxides	Mass, % from Base Case definition (Ibrahim et al, 2023)	Assumed mass in hydration model, mass g/100 g cement
CaO	66.9	66.9
SiO_2	22	22
Al_2O_3	3.3	3.3
Fe_2O_3	2.74	2.74
MgO	0.6	0.6
MnO	<0.02	-*
Na_2O	<0.2	0.2
K_2O	<0.05	0.05
TiO_2	0.18	-*
P_2O_5	0.24	-*
Sulphides	<0.1	-*
Sulphates	2.4	2.4 (SO_3)
Carbon	-	2.1 [26]
Loss to fire (1000 degC)	2.02	-

* - species were not available in thermodynamic database Cemdata18.

The equilibrated porewater composition and mineral phases were derived with thermodynamic model using oxide proportions (Table 4), water cement ratio (0.4275) and curing temperature (20 °C). The set of minerals allowed to form during cement hydration included calcite, portlandite, calcium monocarboaluminate, hydrotalcite, ettringite [26], $C_3FS_{0.84}H_{4.32}$ [27] and CSH. With assumption of 10 % of gas filling the pore volume, derived porosity after hydration was 0.113.

Modelled initial porewater composition of concrete liner is presented in Table 5.

Table 5. Porewater composition of equilibrated cement with water/cement ratio (w/c= 0.4275)

Component	Concentration (mol/L)
Al	1.908×10^{-5}
C	1.629×10^{-5}
Ca	4.845×10^{-3}
Cl	1.280×10^{-7}

Component	Concentration (mol/L)
Fe	2.858×10^{-8}
K	3.902×10^{-3}
Mg	4.746×10^{-9}
Na	7.688×10^{-2}
S	1.416×10^{-4}
Si	3.282×10^{-5}
pH	12.864
pe	6.115

Table 6. Initial solid composition in concrete liner material

Mineral	Amount (mol/m^3 of concrete)
Portlandite	1.59×10^{3}
calcite	1.13×10^{2}
Calcium monocarboaluminate	7.25×10^{2}
$C_3FS_{0.84}H_{4.32}$	6.67×10^{2}
ettringite	3.89×10^{1}
hydrotalcite	1.45×10^{1}
CSH:	1.84×10^{3}
CSHQ-JenD	7.30×10^{2}
CSHQ-JenH:	4.79×10^{2}
CSHQ-TobD:	5.49×10^{2}
CSHQ-TobH:	2.37×10^{1}
KSiOH:	8.09×10^{-3}
NaSiOH:	4.68×10^{-2}

Clayrock porewater composition was based on the information provided in the Base Case definition [25] after charge balance with Phreeqc adjusting solution pH value. The COx porewater composition used in reactive transport modelling is provided in Table 7.

Table 7. COx porewater composition used for simulation

Porewater definition	Porewater derived for simulation

Component	Concentration (mmol/L) defined in (Ibrahim et al., 2023)	Species	Concentration from equilibration (mol/kg water)
Carbonates (Patm)	0.01	C	3.828×10^{-3} equilibrated with partial CO_2 pressure (0.01 P atm)
Chlorure	39.5(±6%)	Cl	3.95×10^{-2}
Sulphate	12.6(±4%)	S	1.26×10^{-2}
Sodium	46.6(±3%)	Na	$4.66e\times10^{-2}$
Calcium	5.4(±8%)	Ca	5.40×10^{-3}
Magnesium	4.5(±6%)	Mg	4.50×10^{-3}
Potassium	0.6(±12%)	K	6.00×10^{-4}
Silice	0.4(±72%)	Si	4.00×10^{-4}
Ammonium	0.2(±30%)	N(-3)	2.00×10^{-4}
pH	7.0±0.3	pH	7.236
		pe	4.0

1.2.3 Mass balance equations

Species and CO_2 could be transported in porous material by advection/dispersion and diffusion in liquid and gaseous phases. It was assumed that during ventilation phase there will be no gas pressure gradient imposed, thus CO_2 transport in gaseous form will be governed by diffusion and dissolved CO_2 will be transported by advection, molecular diffusion and dispersion. No other volatile species were considered in the analysis. Mathematically, species transport could be described by a partial differential equation describing *i* species mass conservation over time in space:

$$\frac{\partial(\theta_l c_i)}{\partial t} + \frac{\partial(\theta_g c_{i,g})}{\partial t} + \mathbf{q_L} \cdot \nabla c_i = \nabla \cdot \left[(D_{D,i} + D_{e,i})\nabla c_i\right] + R_i \qquad (22)$$

where c_i is dissolved species concentration (mol/m^3), $c_{i,g}$ is species concentration in gaseous form (mol/m^3), $\mathbf{q_L}$– Darcy velocity (m/s), $D_{D,i}$ is dispersion tensor (m^2/s) and $D_{e,i}$ is effective diffusion coefficient (m^2/s), R_i is a term describing source or sink of the species (mol/m^{3}s).

In a fully water saturated porous medium, the liquid volume fraction θ_l is equal to porosity *n*, but for an unsaturated medium, it is related to water saturation S_l ($\theta_l = nS_l$). The resulting gas volume fraction in the case of an unsaturated porous medium is

$$\theta_g = n - \theta_l = (1 - S_l) \cdot n \qquad (23)$$

Components of dispersion tensor are:

$$D_{Dii} = \alpha_L \frac{q_{Li}^2}{|q_L|} + \alpha_T \frac{q_{Lj}^2}{|q_L|} \qquad (24)$$
$$D_{Dij} = (\alpha_L - \alpha_T) \frac{q_{Li} \cdot q_{Lj}}{|q_L|}$$

Where D_{Dii} is diagonal components of dispersion tensor (m²/s), D_{Dij} is off diagonal components of dispersion tensor (m²/s), α_L and α_T are longitudinal and transverse dispersivities (m).

Effective diffusion coefficient $D_{e,i}$ for solutes in porous media was described as a function of liquid volume fraction, tortuosity:

$$D_{e,i} = D_{L,i} = \theta_l \tau D_o \tag{25}$$

where τ is the medium tortuosity. For partially saturated porous media, tortuosity is related to water content through relationships such as [7]:

$$\tau = \frac{\theta_l^{7/3}}{n^2} \tag{26}$$

According to Henry's law, the concentration of CO_2 in gas phase is linearly related to dissolved CO_2 concentration:

$$c_{CO2,g} = \frac{c_{CO2,d}}{H} \tag{27}$$

here H is Henry's constant for CO_2 (dimensionless).

Then for CO_2, effective diffusion coefficient could be expressed as follows:

$$D_{e,CO2} = D_{L,CO2} + \frac{1}{H} D_{G,CO2} \tag{28}$$

CO_2 diffusivity in gas phase was described as:

$$D_{G,CO2} = \theta_g \tau_g D_g^f \tag{29}$$

where D_g^f is the diffusion coefficient of the f-th gas species in an ideal gaseous phase which according to [28] is given by:

$$D_g^f = \frac{RT}{3\sqrt{2}\pi P N_{avog} d^2} \sqrt{\frac{8RT}{\pi M}} \tag{30}$$

where P is the gaseous phase pressure, N_{avog} is Avogadro's number, and d and $M$are the molecular diameter and the molecular weight of the f-th gas species, respectively. The tortuosity in the gaseous phase (τ_g) is computed from [7]:

$$\tau_g = \frac{\theta_g^{7/3}}{\mathrm{n}^2} \tag{31}$$

With molecular diameter of the gases species 10^{-10} (m), D_g^f is 1.17×10^{-4} m²/s. For material with relative humidity of 60 %, effective diffusivity in gaseous form was estimated 3.5×10^{-7} m²/s.

1.2.1 Water flow

Modelling of hydro-chemo-mechanical processes considered: advective water flow including relative permeability's and capillary pressure depending upon liquid saturation; advective/dispersive dissolved CO_2 and gas diffusive transport of CO_2 ; aqueous complexation, advective/dispersive transport of dissolved species (solutes); dissolution/precipitation of minerals; poroelasticity and evolution of material stiffness due to chemical damage.

Groundwater flow conditions around the tunnel were simulated solving Richard's equation for unsaturated flow with assumption of constant total gas pressure. Water mass ($m_w = \theta_l \rho_w$) balance equation was solved with finite element method:

$$\frac{\partial m_w}{\partial t} + \nabla(\rho_w \mathbf{q}_L) = Q \tag{32}$$

Where $\mathbf{q}_L$ is advective flowrate of water, Q is water sink/source.

The advective flowrate for liquid phase was described by extended Darcy law:

$$\mathbf{q}_L = -\frac{k_w k_{rw}}{\mu_w}(\nabla P_L + \rho_w \mathbf{g}) \tag{33}$$

where k_w, k_{rw} are intrinsic and relative permeability of the porous material respectively (m^2 and unitless), P_L is water pressure (Pa), $\mathbf{g}$ is gravity (m/s^2), ρ_w is water density (kg/m^3).

Relative permeability is a function of effective saturation, which is evaluated from material's water retention curve (WRC). Van Genuchten water retention curve was considered in this study:

$$S_e = \frac{1}{(1 + (\alpha_{VG} s_M)^{n_{VG}})^{m_{VG}}}, \qquad \text{for } s_M > 0, \text{otherwise } 1 \tag{34}$$

$$\theta_l = \theta_r + S_e(\theta_s - \theta_r), \qquad for\ s_M > 0, \text{otherwise } \theta_s \tag{35}$$

$$k_{rw} = (S_e)^l \left[1 - \left(1 - S_e^{\frac{1}{m_{VG}}}\right)^{m_{VG}}\right]^2, \qquad \text{for } s_M > 0, \text{otherwise } 1 \tag{36}$$

$$s_M = P_g - P_l \tag{37}$$

Where S_e is effective saturation (-), s_M is suction (capillary pressure) (Pa), α_{VG} (1/Pa), n_{VG}, m_{VG}, l, θ_r are Van Genuchten WRC model parameters. θ_r, θ_s are residual and saturated water content.

1.2.2 Poro Mechanical aspects

For mechanical analysis, all materials were assumed to be poroelastic materials. Mechanical force balance equation was defined:

$$\nabla \cdot \boldsymbol{\sigma} = -\mathbf{F_v} \tag{38}$$

where $\boldsymbol{\sigma}$ is total stress tensor, $\mathbf{F_v}$– body force ($kg/(m \cdot s^2)$). Gravity was not considered in the analysis, thus $\mathbf{F_v}$=0. The strains in porous material are caused by effective stresses described as follows:

$$\sigma_{ij}' = \sigma_{ij} - \alpha \cdot \bar{P} \tag{39}$$

$$\bar{P} = S_l \cdot P_l + (1 - S_l) \cdot P_g = P_g - S_l \cdot s_M \tag{40}$$

$$\alpha = 1 - \frac{K_D}{K_g},\ K_g = \frac{K_D}{1-\alpha} \tag{41}$$

Where σ_{ij} and σ_{ij}' are total and effective stress (Pa) respectively, α is Biot coefficient (-), $\bar{P}$ is equivalent pore pressure (Pa), K_D is drained bulk modulus of the material (Pa), K_g is solid (grain) bulk modulus (Pa).

It was coupled to unsaturated flow model via definition of effective stress and considering strains induced water source Q_{HM} as well as (S), the derivative of the water retention curve, and moisture capacity (C_m):

$$\frac{\partial m_w}{\partial t} = \rho_w S_l S \frac{\partial (P_L)}{\partial t} + n\rho_w C_m \frac{\partial P_L}{\partial t} + Q_{HM} \quad (42)$$

Assuming isothermal conditions (T=23 °C) and constant gas pressure ($P_g = 0.1$ MPa), derived terms for water mass change over time in poroelastic material:

$$S = n\beta_{lP} + S_l \frac{(\alpha - n)(1 - \alpha)}{K_D} \quad (43)$$

$$Q_{HM} = S_l \alpha \frac{de_v}{dt} \quad (44)$$

$$C_m = \frac{\partial (S_l)}{\partial P_L} = \left(1 - \frac{S_l s_M}{n} \frac{(\alpha - n)(1 - \alpha)}{K_D}\right) \quad (45)$$

where *n* is porosity, e_v is volumetric strain (-), β_{lP} is water compressibility (1/Pa).

In parallel, a separate partial differential equation has been solved for CO_2 transport in concrete and EDZ which provide the input (partial pressure of CO_2) to chemical solver. CO_2 transport was performed in EDZ as the later could be unsaturated and CO_2 concentration in it could be different than that of fully saturated COx clay rock (0.01 atm).

1.2.3 Chemo mechanical coupling

Chemical degradation of concrete was simulated using mass conservation law (mass action law) and all the reactions were assumed at chemical equilibrium, where activities of the species are related though the equilibrium constant K [29]:

$$K = \frac{\prod_{products} a_p^{\nu_p}}{\prod_{reactants} a_r^{\nu_r}} \quad (46)$$

where $a_p^{\nu_p}$ and $a_r^{\nu_r}$ are activities and ν_p and ν_r are stoichiometric coefficients of the products and reactants, accordingly.

With chemical solver, the evaluation of mineral volume changes and changes of Ca in concrete solid skeleton were done too. Changes of mineral volumes were converted into porosity changes:

$$n = 1 - V_{minerals} - V_{inert} \quad (47)$$

where $V_{minerals}$ is the volume of minerals in 1 m^3 concrete, V_{inert} the volume of inert materials in 1 m^3 concrete.

The chemical damage due to leaching was considered as a scalar variable and affects the Young's modulus as a function of calcium content in the concrete solid skeleton [30].

$$E = E_0(1 - d_c) \quad (48)$$

$$d_c = d_{c,max}\left[1 - e^{\left(Ca^{solid} - Ca_0^{solid}\right)}\right] \quad (49)$$

where $d_{c,max}$ is asymptotic values of chemical damage, Ca_0^{solid} is initial (in sound condition) concentration of calcium in the solid skeleton; and Ca^{solid} is actual concentration of calcium in the solid skeleton.

Modelling of coupled HMC processes in predefined system required revision of the mathematical model for unsaturated flow in poroelastic material and definition of coupling terms. Porosity change due to

dissolution/precipitation of minerals in concrete material and its impact on solute diffusivity was taken into account dynamically.

1.3 Reactive transport model of CSIC

The model CheProf has been selected to simulate and assess the evolution of mineral phases over time near the concrete-rock interface, potentially resulting in variations in porosity. A brief overview of the used code and the performed model is described.

1.3.1 CheProf model

The code CheProf (CHEmical PROcesses Object-oriented with Fortran 2003) calculates reactive transport in a one-dimensional domain discretized by finite elements. It is developed by the Hydrogeology Research Group (GHS) from the Department of Civil Engineering at the Technical University of Catalonia (UPC) based on numerous studies [31], [32], [33], [34], [35].

The code serves the dual functionality of reading and writing input files using Phreeqc simulations and a defined thermodynamic database. The input data is structured in ChemSys and LocalChem files, where "ChemSys" contains all chemical equations of state, such as mass action laws, kinetic rate laws, definition of components, phase constraints and activity models, while "LocalChem" refers to chemical state variables, such as temperature, concentrations of all species and volume fractions of phases.

Activities within the chemical systems can be modeled assuming ideal mixtures or using the extended Debye-Hückel (1923) [36] equation; reactions can be equilibrium-based, following the mass action law, or kinetic in nature. Finally, the code uses the Newton-Raphson method to solve reactive transport presenting a comprehensive solution for modeling complex chemical systems and transport phenomena.

Since the elaboration of the model requires a source of input information and the available experimental data is scarce, different sources have been chosen to select the data which will lead us to simulate the evolution of the chemical system.

The studies conducted at the Mont Terri Underground Rock Laboratory have been considered, in particular, those related to the Cement-Clay Interaction (CI and CI-D) experiment [37]. The results of this experiment and previous studies that lay the groundwork for the development of related reactive transport models established the basis for the development of this approach. As assumed in the hydro-mechanical HM model, the material defining the concrete support structure is characterized by Portland cement and the rock characteristics come from Opalinus Clay formation.

1.3.2 Thermodynamic data

The chemical equilibrium constants (25 ºC) is listed in Table 8. The definition of equilibrium reactions and the corresponding equilibrium constants for equilibria in solution were taken from the Thermo-Chimie version12a database. The activity of water was taken to be equal to 1. Equilibrium constants for the solubility of the solid phases are also taken from the mentioned database.

Table 8. Equilibrium constants (log K_{eq} 25ºC) for solution and mineral reactions

Species	**log K_{eq}**	**Species**	**log K_{eq}**
$Ca(H_3SiO_4)^+$	-8.83	$Na(CO3)^-$	1.27
$Ca(HCO_3)^+$	11.43	Na(HCO3) (aq)	10.08
$Ca(OH)^+$	-12.78	Na(OH) (aq)	-14.75
$CaCl^+$	-0.29	NaCl (aq)	-0.50
$CaCO_3$ (aq)	3.22		
CO_2 (aq)	16.68	**Minerals**	**log K_{eq}**
$H_2(SiO_4)^{-2}$	-23.14	Calcite	-8.83
$H_3(SiO_4)^-$	-9.84	CSH1.6	11.43
HCO_3^-	10.33	CSH1.2	-12.78

K(OH) (aq)	-14.46	CSH0.8	-0.29
KCl (aq)	-0.50	Portlandite	3.22

Effective diffusion coefficients (D_e) in each part of the model domain is calculated according to

$$D_e = \emptyset D_0 \quad (1)$$

where $\emptyset$ is porosity and D_0 a reference diffusion coefficient (constant for the whole model domain). Since $\emptyset$ changes along the model domain and through time due to the dissolution and precipitation of solid phases, D_e changes linearly with $\emptyset$.

The initial D_e value of 4.0x10^{-11} m^2/s for concrete in the model corresponds to the calibrated transport model calculated in Soler (2022) [37].

It has been defined a hypothetical problem that simulates the interaction between a support concrete structure and the confining rock in a deep waste repository. To quantify the potential effect of reaction-induced concrete degradation, it has been decided to address the problem separately: on the one hand, the hydro-mechanical (HM) problem; and on the other hand, the hydro-chemical (HC) problem. The subsequent task involves integrating these models into a HCM model determining an appropriate coupling method that allows us to analyse the possible alteration on concrete.

2. Applications to the Base Case study

The different chemo-mechanical models developed in Task 4 were then all applied to a common study case, called a "base case", the definition of which was the subject of a specific report [25].

This base case represents a 100,000-year study of the chemomechanical behavior of a concrete tunnel subjected to mechanical pressure induced by the surrounding rock, as well as to chemical perturbations induced by the water contained in this rock (with little mineralization) and the atomsphere inside the tunnel (with CO2).

2.1 Base case interpretation for Andra-LMDC

The chemical calculation of the base case study considers the phenomenon of calcium leaching occurring on the extrados in contact with host rock, and atmospheric carbonation on the intrados of a tunnel structure. These two chemical degradations were applied as boundary conditions to the tunnel walls, in addition to the moisture condition that changed over the tunnel's lifetime.

2.1.1 Dimensions

The mesh for chemical calculations is simplified along two symmetrical axes. The section studied is limited to a quarter of the tunnel cross-section. For the meshing, a 50 cm length of the concrete is discretized along the unidirectional path of degradation enabling us to project our results onto the entire cross-section (Figure 2.1). The utilization of a refined mesh is necessary for the chemical calculations in this study in order to capture the species diffusion and the change of concentrations at short times. This approach optimizes computational efficiency while maintaining the accuracy of our analysis of the tunnel's structural response to degradation. For the mechanical calculation, the mesh used is the quarter of the tunnel due to the symmetry with respect to the two axes of the plane (Figure 2.2).

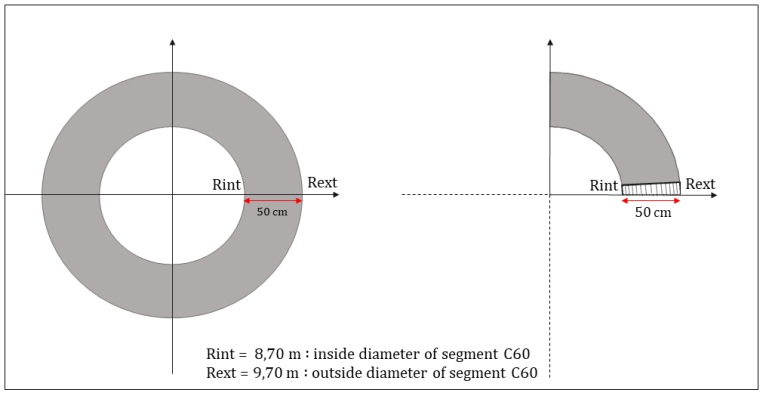

Figure 2.1 : Cross section of the base case and the mesh used for the chemical calculation

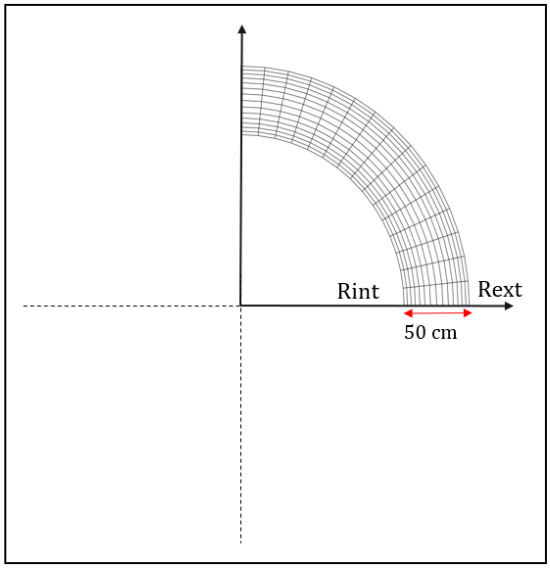

Figure 2.2 : Mesh used for the mechanical calculation

2.1.2 Initial and Boundary conditions:

A. Chemical calculation

At the Extrados

At the extrados of the tunnel, decalcification is anticipated due to contact with groundwater. The concentrations of the calcium in the host rock is 5.4 mol/m^3. Moreover, the soil pore water contains a concentrations of dissolved carbon dioxide corresponding to $P_{CO2} = 0.01\% \, Patm$. The degree of water saturation of the extrados starts with an initial partial water saturation of 80% and increases until saturation is reached.

At the Intrados

The tunnel intrados will be subjected to atmospheric carbonation for the first 100 years, at constant relative humidity. After closure of the tunnel, the concrete structure will resaturate from the extrados to the intrados. Two Dirichlet boundary conditions are applied. The first is imposed to the maximum concentration of carbon dioxide corresponding to $P_{CO2} = 0.04\% \, Patm$ that can diffuse into the concrete. The second is the degree of water saturation, which starts with a constant initial value with 50% until 100 years. Later, it varies over time to reach full saturation of the tunnel after 10,000 years [38].

B. Mechanical calculation

A first chemical calculation of the base case was performed at constant temperature using the thermo-hydro-chemical model described in chapter 1. Then, at each time step, the elastic modulus is

determined through the homogenization scheme in the section 1.1.3. Thus, the mechanical behaviour of the tunnel is predicted using the mechanical model of LMDC under a constant pressure of host rock of 4 MPa on the structure. This pressure is applied as a load on the extrados of the tunnel and is constant over time. The mechanical boundary conditions correspond to the symmetry axes of the geometry (figure 2.2).

2.1.3 Results

A. Chemical results

The chemical model was used to simulate a duration of a million years. The time step used increases over time according to the convergence of the model, and the duration of the calculations was approximately 40-45 days. The Figure 2.3 shows the field of remaining calcium bound in solid during leaching at different milestones. Even after one million years, the concrete is not completely decalcified due to the presence of calcium in solution in the host rock at a concentration of 5.4 mol/m^3 (corresponding to a residual amount of calcium in solid phase equal to 1180 mol/m^3). Carbonation remains slow (only a few cm at intrados) due to the change in the hydrous state and to the clogging effect of formed calcite as illustrated in Figure 2.4. When evolving to a saturated medium, diffusion of gaseous CO_2 decreases and the rate of carbonation decreases. The calcite profile is given in the Figure 2.4. The result of this chemical calculation enabled us to obtain the volumes of the phases in order to apply the homogenisation scheme allowing the assessment of mechanical properties at each time step.

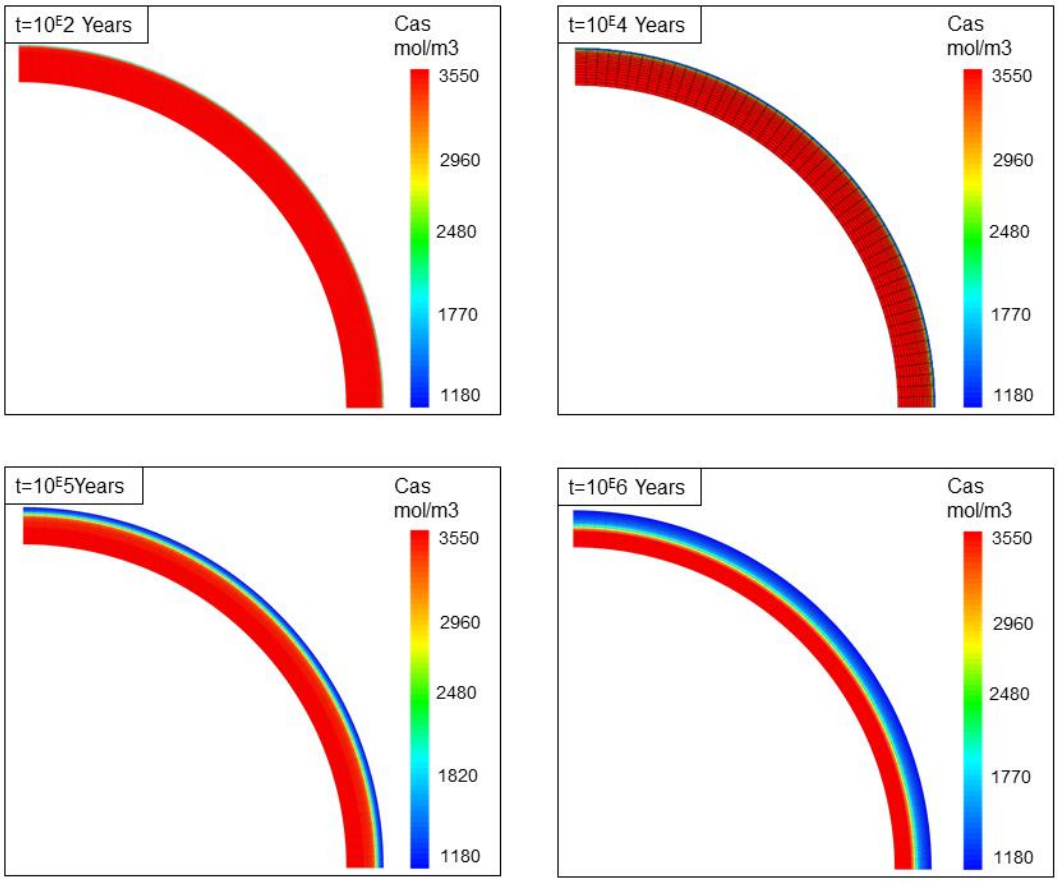

Figure 2.3 : fields of calcium in solid phase at different times: calcium leaching at the tunnel extrados reaches the mid-depth of the concrete wall at one million years (LMDC model) *(note 'Cas' corresponds to Calcium in solid phase)*

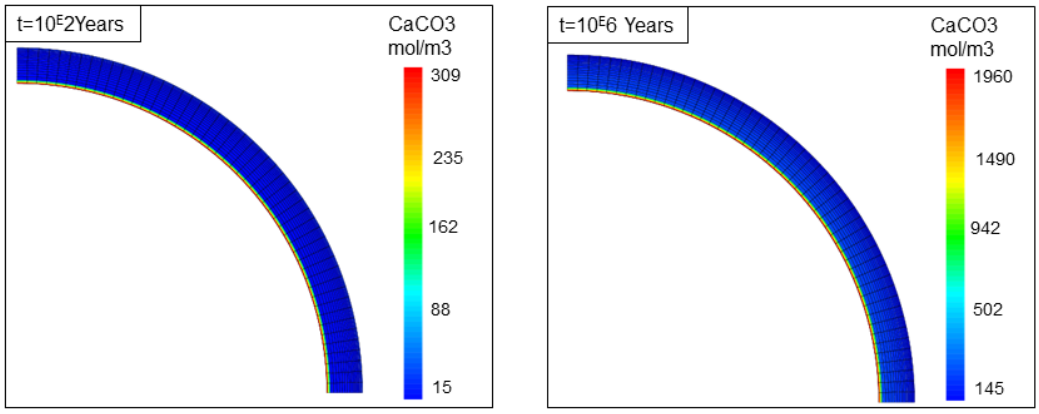

Figure 2.4 : The field of precipitated calcite at different times due to atmospheric carbonation in the tunnel intrados and decalcification due to groundwater in the tunnel extrados (LMDC model)

B. Mechanical results

The homogenisation scheme explained in section 1 has been applied following the chemical calculation. The fields of elastic young's modulus are shown in Figure 2.5 at different times. The Young's modulus of concrete depends on its chemical evolution. We can observe that decalcification leads to a decrease in elastic modulus due to the dissolution of hydrates at the tunnel extrados. On the other hand, at the intrados of the tunnel, there is an increase of this modulus due to the precipitation of calcite resulting from concrete carbonation.

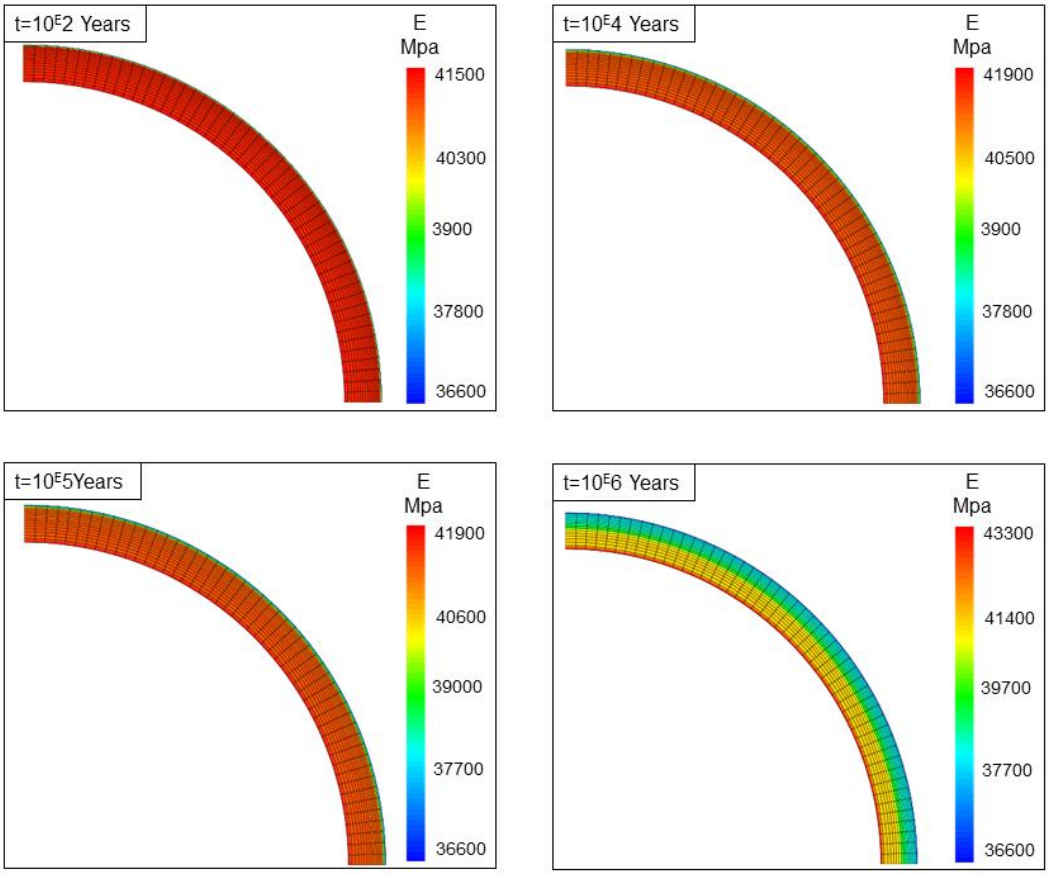

Figure 2.5 : Prediction of the fields of elastic Young's modulus at different times of chemical degradation (LMDC model)

After calculating the elastic properties of the concrete, the poromechanical model is applied to calculate the deformation of the tunnel under the ground stress. After one million years under a soil pressure assumed to be equal to 4 MPa, there is a radial convergence of 3 cm (Figure 2.6). The stress field in

the concrete are shown in Figure 2.7. The effect of leaching on the outer edge of the tunnel is well reproduced by the model, represented by a reduction in stresses in this zone. This model could also be used to determine when the tunnel will collapse under a given stress, or under a controlled convergence of the host rock. To achieve such calculation, a realistic behaviour law of the host rock should be coupled to this thermo-hydro-chemo-mechanical model.

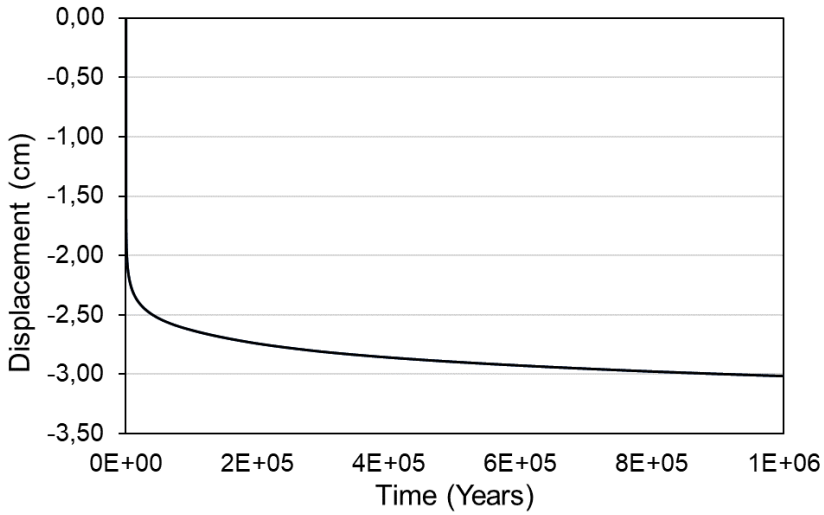

Figure 2.6: Displacement of the tunnel intrados over time (LMDC model)

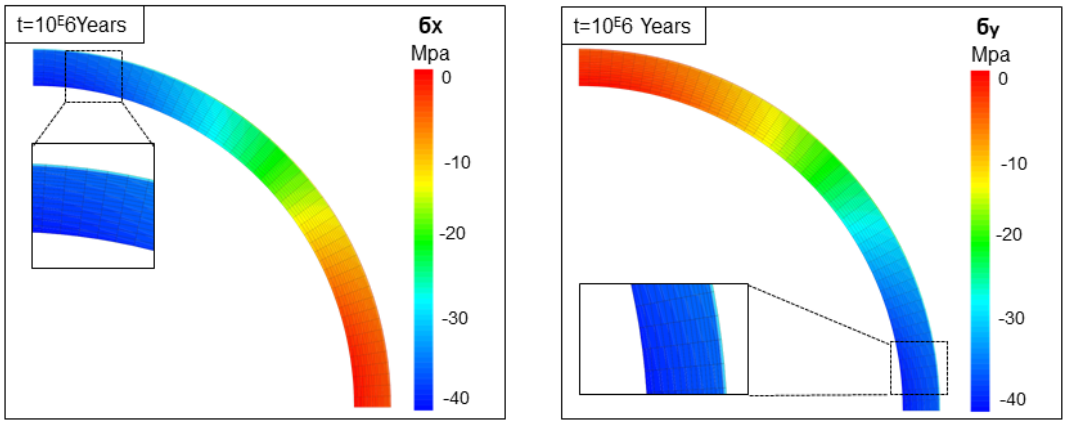

Figure 2.7: The stress fields after 10^6 years of chemical degradation and radial pressure of 4 MPa induced by host rock (LMDC model)

2.2 Base case interpretation for LEI

Model for Base case considered three different materials: concrete liner, excavation disturbed zone (EDZ) and part of the host rock (Callovo-Oxfordian clay rock) following Base Case definition [25].

The different HMC processes related parameters required for the reactive transport simulations are summarized up in Table 9

Table 9: Parameters required for the reactive transport simulations

Parameters	Concrete	EDZ	COx
Hydraulic			
Intrinsic permeability (m^2)	7.3×10^{-20} [39]	1×10^{-16} [25]	1×10^{-20} [25]
Water retention parameters: α_{VG} (1/Pa) n_{VG} m_{VG} l	[39] 2×10^{-8} 1/Pa 2 0.5 0.5	[40] 2.6×10^{-8} 1/Pa 1.8 0.45 0.5	[40] 2.6×10^{-8} 1/Pa 1.8 0.45 0.5

θ_r	0	0	0
Relative permeability	Van Genuchten model		
Saturated volumetric water content (-)	0.113	0.15 [25]	0.15 [25]
Porosity (-)	0.113	0.15 [25]	0.15 [25]
Transport			
Water density (kg/m^3)	1×10^3		
Molecular diffusion in water inside concrete D_o (m^2/s)	2×10^{-11}		
Liquid viscosity (Pa.s)	1×10^{-3}		
Molecular diameter of gas species (m)	1×10^{-10}		
Mechanical			
Young modulus (MPa)	42 [25]	$0.75\times E_{Cox}$ [25]	5400 [25]
Poisson ratio (-)	0.28 [25]	0.29 [25]	0.29 [25]
Biot coefficient (-)	0.2	0.6 [25]	0.6 [25]
Initial Ca in solid skeleton (mol/dm^3 of concrete)	4.86	-	-
Maximum damage (-)	0.7 [30]	-	-

2.2.1 Dimensions

A 2D numerical model for the Base case was developed. In a tunnel of 9.7 m diameter, a 0.5 m thick concrete liner was defined. The model contains excavation disturbed zone of anisotropic dimensions (10 m x 15 m). Half of the liner, EDZ and the host rock was modelled considering symmetry for the whole liner. The extension of the model in horizontal direction corresponds to half the distance between disposal tunnels (50 m), the model dimensions in vertical direction was 120 m (Figure 2.8).

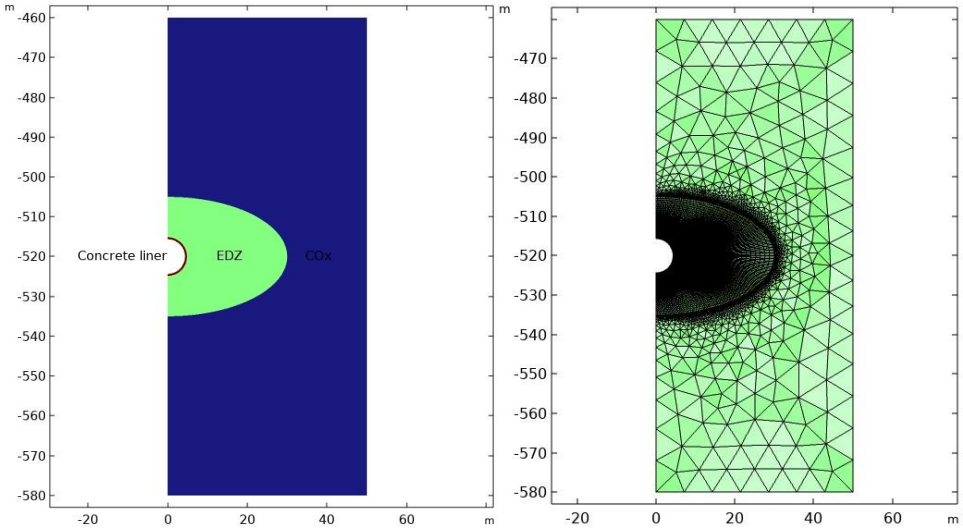

Figure 2.8: 2D model geometry considered for the analysis: brown – concrete liner, green – EDZ, blue – COx clayrock

The modelling domain was discretized into quadratic and triangular mesh elements (~15000).

2.2.2 Initial and boundary conditions

The following initial and boundary conditions were assumed (see also Figure 2.9):

- Tunnel excavation was represented by reducing the load at tunnel wall linearly within 1 day.
- On model top (DC line in Figure 2.9) and right boundary (BC line in Figure 2.9) load was set equal to in situ stress (σ_v=13.4 MPa, σ_h=13.1 MPa).

- Zero normal displacement boundary condition was set on the boundaries AE', ED, AB, BC (see Figure 2.9).
- Concrete liner installation was modelled as instant material activation after 4 days.
- At emplacement, concrete liner is not fully water saturation (58 %), while EDZ and COx were assumed to be fully saturated.
- The initial porewater pressure in EDZ and COx was set equal to 5.3 MPa.
- Porewater pressure was set constant (5.3 MPa) on top (DC), right (BC) and bottom model boundaries (AB), gravity was not considered.
- During ventilation phase from 4 days till 100 years the constant suction (-70 MPa) was imposed on concrete liner inner boundary (EE') to represent relative humidity 60 % as defined in Base Case definition.
- After 100 years, the Dirichlet boundary condition (fixed suction) was changed to no-flow boundary condition (EE').
- For CO_2 transport analysis, the Dirichlet type boundary conditions were applied: at inner concrete wall (EE') partial CO_2 pressure was fixed to be equal to 0.032% atm (log pCO2=-3.5), while on the outer EDZ boundary (FF') it was fixed to be equal to 0.01% atm (log pCO2=-2) as provided for COx clayrock (Table 7).
- Fixed CO_2 partial pressure on the inner concrete wall (EE') was from 4 days-100 years, then it was changed to no-flow boundary condition.
- For solute transport, fixed concentration boundary conditions were set on concrete inner wall and on EDZ outer boundary (COx porewater composition).
- Fixed solute concentration on the inner concrete (EE') wall was from 4 days-100 years, and then it was changed to no-flow boundary condition.

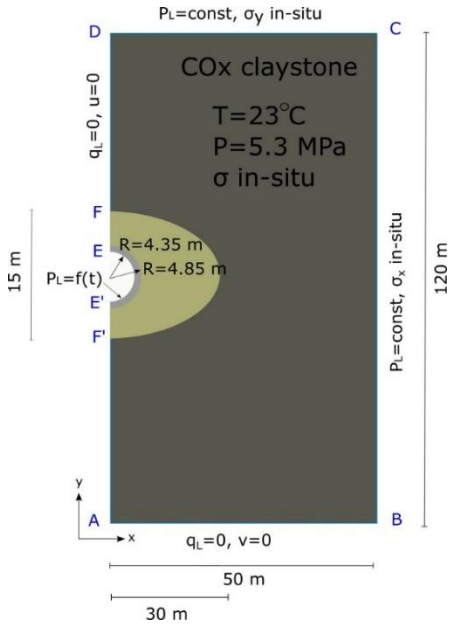

Figure 2.9: Initial and boundary conditions for HM processes

2.2.3 Results

For the analysis of the hydromechanical-chemical, evolution of the concrete liner in disposal tunnel excavated in COx clayrock several cases were defined. Firstly, the evolution of pore pressure and gas pressure around the deposition tunnel was analysed without chemical reactions. Then reactive transport simulations were constrained and coupled to HM model.

2.2.3.1 Pressures

Figure 2.10 present the porewater flow conditions around the tunnel. Modelling results showed that with assumed material hydraulic properties, water retention properties, the EDZ surrounding disposal tunnel became unsaturated during the ventilation phase (full duration of 100 years). The extent of unsaturated conditions increases gradually approximately up to EDZ outer boundary. Once the ventilation has finished, the EDZ started to re-saturate.

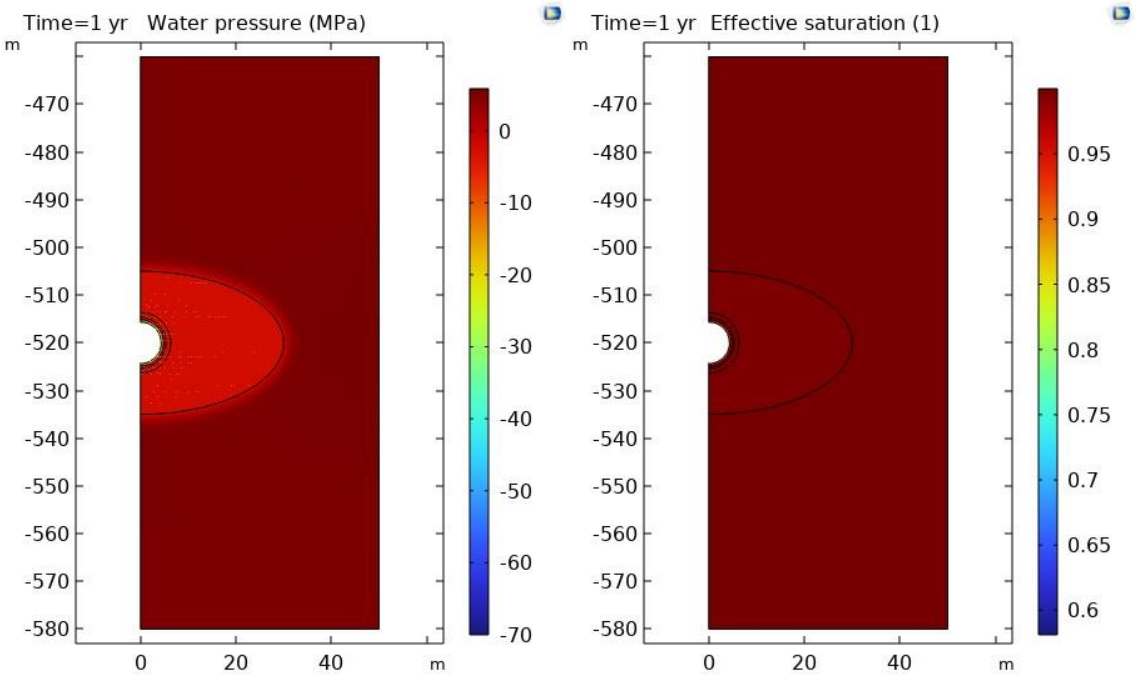

a)

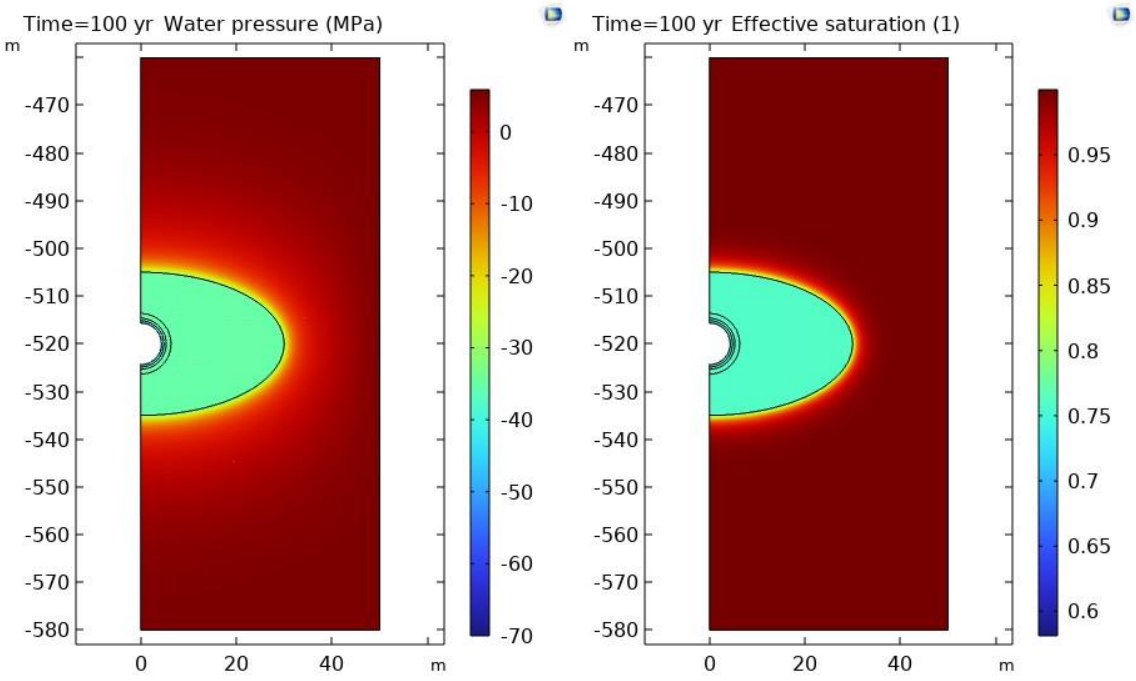

b)

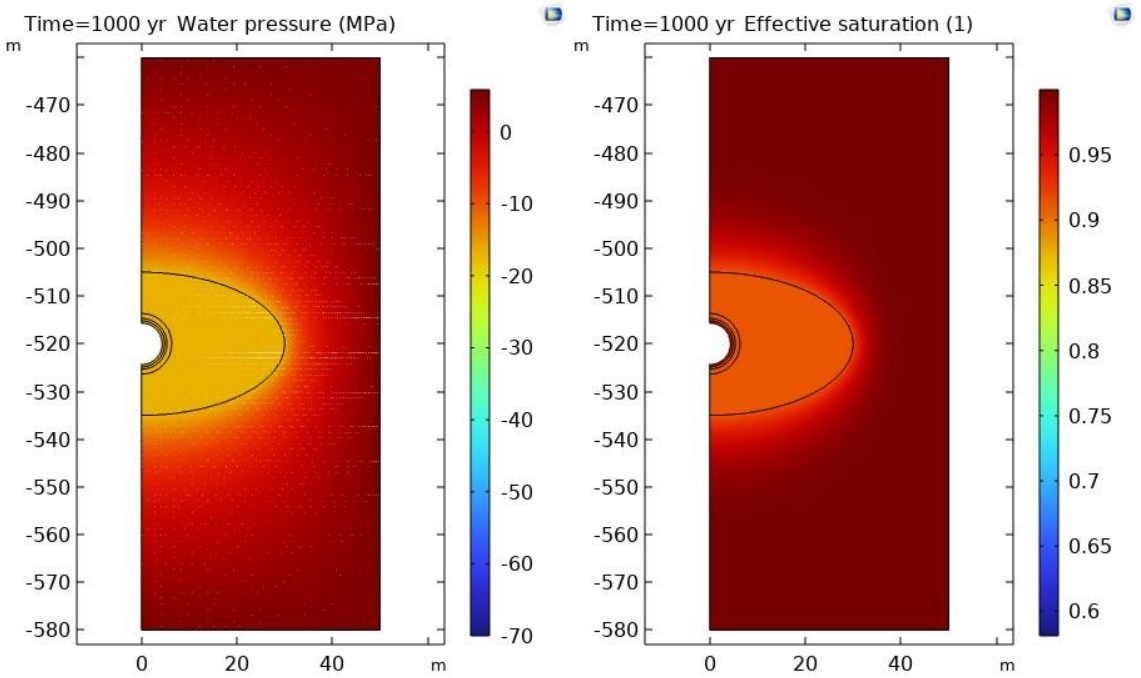

c)

Figure 2.10: Porewater flow conditions (liquid pressure and effective saturation) around the tunnel at different times after excavation: a) 1 year, b) 100 years, c) 1000 years

The unsaturated conditions resulted in a situation where CO_2 in gaseous form could be easily transported in the concrete and EDZ. Its dissolution in the porewater was considered via Henry's law. Gaseous diffusivity is much faster than that of dissolved CO_2, thus it governs the total CO_2 mass transport. Due to imposed gradient in CO_2 partial pressure towards tunnel (pCO_2=0.00032 atm at r=4.35 m and pCO_2=0.01 atm at r ranging from 10 to 15 m in vertical and horizontal directions), the certain profile of CO_2 across the concrete and EDZ was established by the end of ventilation phase (Figure 2.11).

CO_2 transport modelling results showed that CO_2 partial pressure in the concrete under unsaturated conditions would be lower than that imposed by saturated COx porewater. After, ventilation finished and there is no fixed CO_2 pressure on the concrete liner inner boundary, CO_2 equilibrated very quickly across the liner.

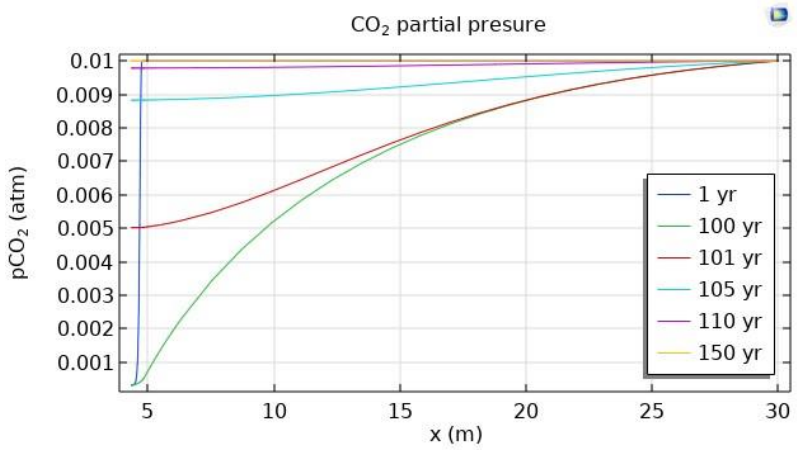

Figure 2.11: CO_2 partial pressure profile at tunnel at different times after excavation

To specify evolutions in concrete, Figure 2.12 gives somes locations where evolutions of saturation and pH are commented below. Figure 2.13 gives the water saturation evolution across the concrete at different date, and Figure 2.14 the saturation evolution versus time at the different locations specified in Figure 2.12.

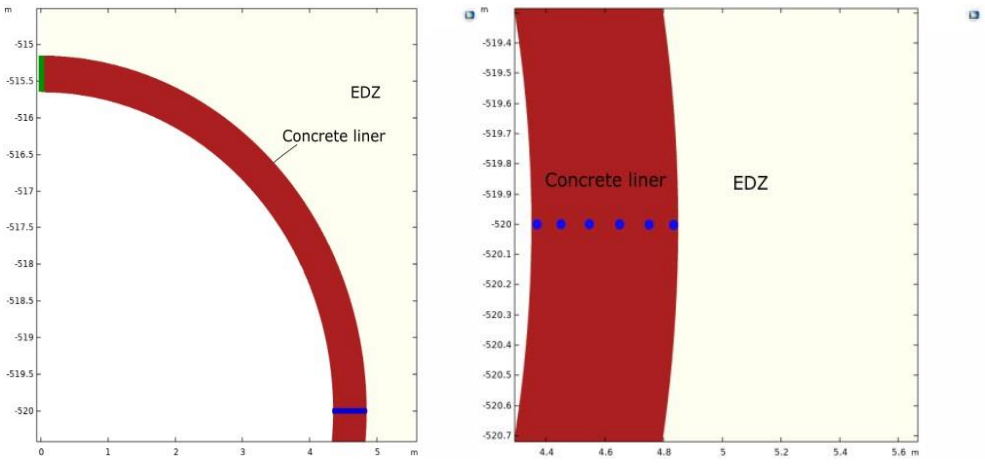

a) b)

Figure 2.12: Positions, selected for the observations of the changes in effective saturation and pH over liner: blue line – in the horizontal direction, green line – in the vertical direction (a); points at different distance from liner-EDZ interface (at 1 cm, 10 cm, 20 cm, 30 cm, 40 cm, 49 cm) (interface is located at tunnel radius R=4.85 m) (b)

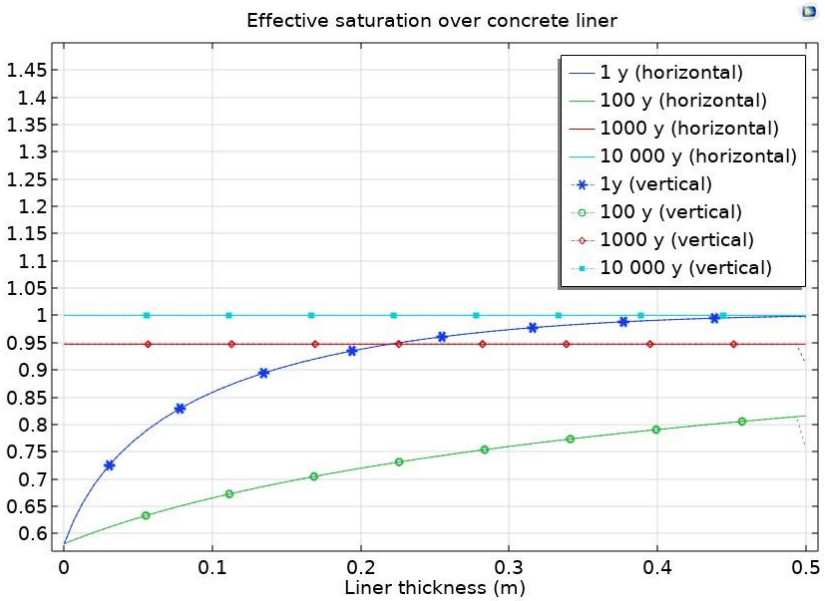

Figure 2.13: Evolution of concrete saturation (vertical axis) over the concrete liner of 50 cm thickness (from liner inner wall) in horizontal and vertical direction

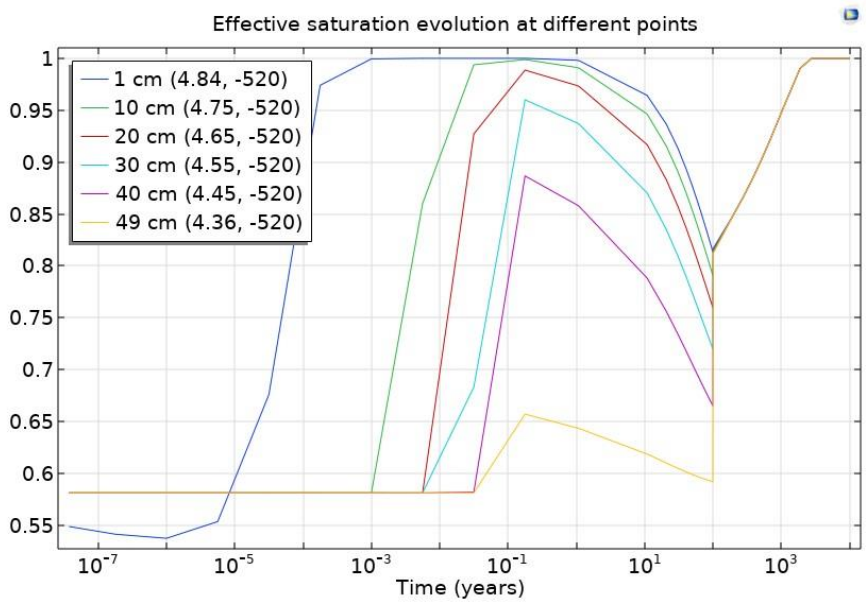

Figure 2.14: Effective saturation evolution in points at different distance from concrete liner-rock interface (at 1 cm, 10 cm, 20 cm, 30 cm, 40 cm, 49 cm from liner-rock interface)

The long terme desaturation of concrete illustrated in Figure 2.13 and Figure 2.14 describes the progression of carbonation, that could affect the stability of reinforcement due to th pH evolution induced. This point will be discussed below.

2.2.3.2 Chemical results

During reactive transport modelling, the CO_2 interaction with the concrete porewater and its minerals was considered, leading to concrete carbonation. In addition, leaching of concrete has been taken into account as the transport of solutes was simulated too. The advective/dispersive transport equation was solved for a number of species specified in the concrete and COx porewater. During carbonation calcite may precipitate. Portlandite and other cement minerals are dissolving/precipitating depending on the prevailing conditions. Mineral precipitation/dissolution was considered only in the cement meshed region and disregarded in the clay rock (EDZ and undisturbed COx). Reactive transport simulations were performed in the concrete and the EDZ where the composition of coming rock porewater were affected by the ventilation. Meanwhile HM processes were simulated over the whole model domains. Modelling such a complex system is high computational resources demanding task. Within this study, the simulations were done up to 10 000 years.

Figure 2.15 presents the pH distribution in the modelled system over time.

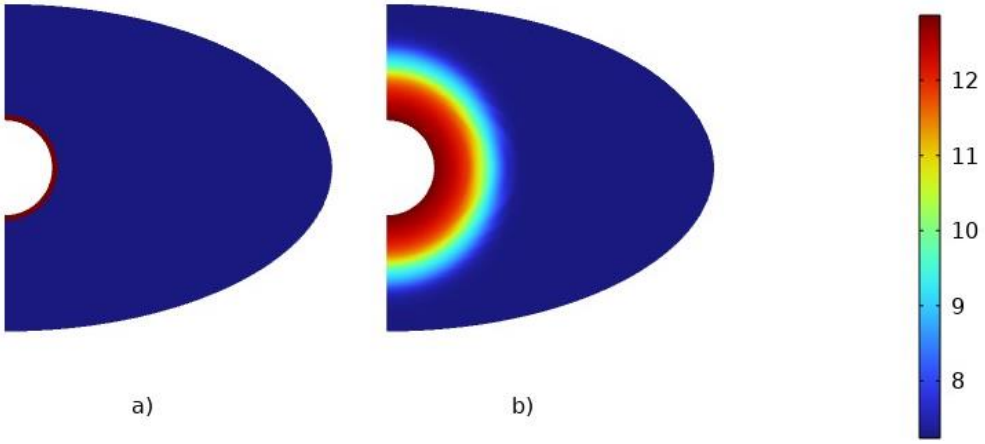

Figure 2.15: pH distribution around the tunnel at different times: a) at 0 year, b) at 10 000 years

Simulation results indicate that the higher pH zone is not restricted to the concrete liner only. It propagates into the EDZ. Once the system became re-saturated again and without imposed regional groundwater flow, the transport was calculated to be diffusion dominated. This is indicated by symmetrical pH distribution from the liner. According to [41], the corrosion initiation of rebars embedded in the concrete can occur when the pH is between 11.3 and 12.1. Within modelled time period, porewater pH decrease (to pH~11 and lower) in the host rock but not so much in the concrete region. So the corrosion of the reinforcement would not be expected. Subsequently, it should not impose the chemical degradation of rebars in the concrete and reduction of the mechanical strength of the structure. pH distribution is related to the distribution of Na, K concentrations in the pore water. Figure 2.16 presents the distribution of mentioned elements initially and by the end of simulation (10 000 years). As it could be seen, Na and K are slowly transported from the liner into the EDZ.

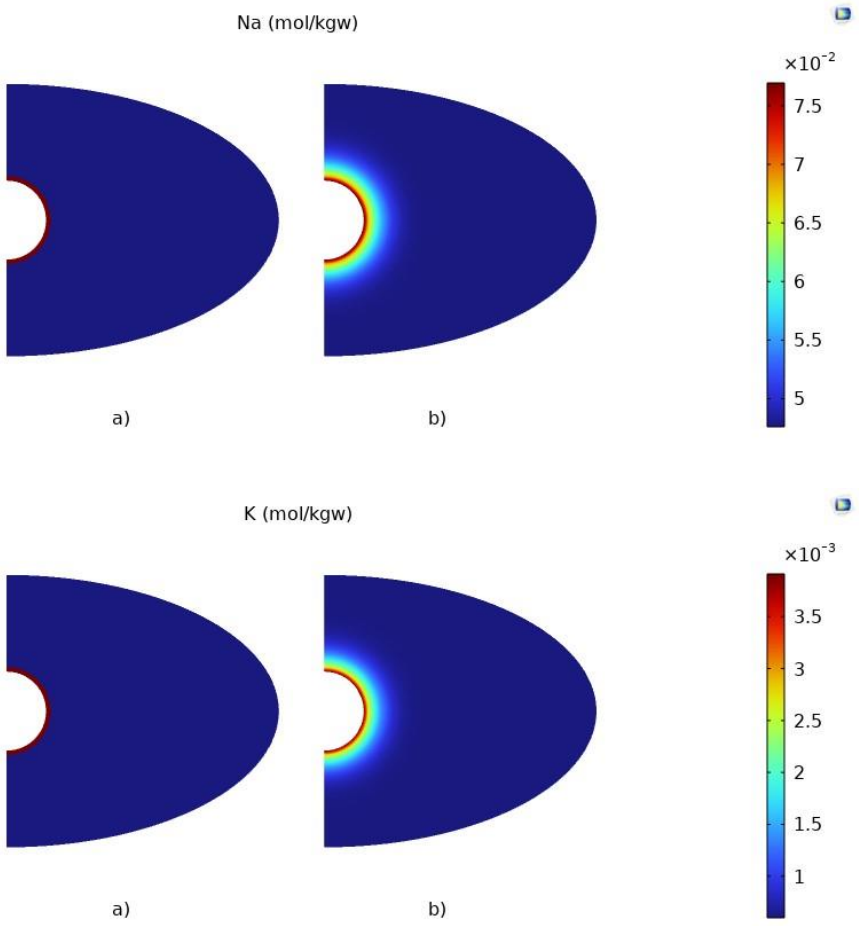

Figure 2.16: distribution of Na, K concentrations in the pore water of modelled system a) at 0 year, b) at 10 000 years.

Dissolution and/or formation of the minerals in the analysed system proceed very slowly. The extent of portlandite dissolution and calcite precipitation was limited and was related to the outer part of the liner as it was expected because of higher pCO_2 on the outer liner boundary. Figure 2.17 to Figure 2.23 show mineral concentrations initially and by the end of simulation.

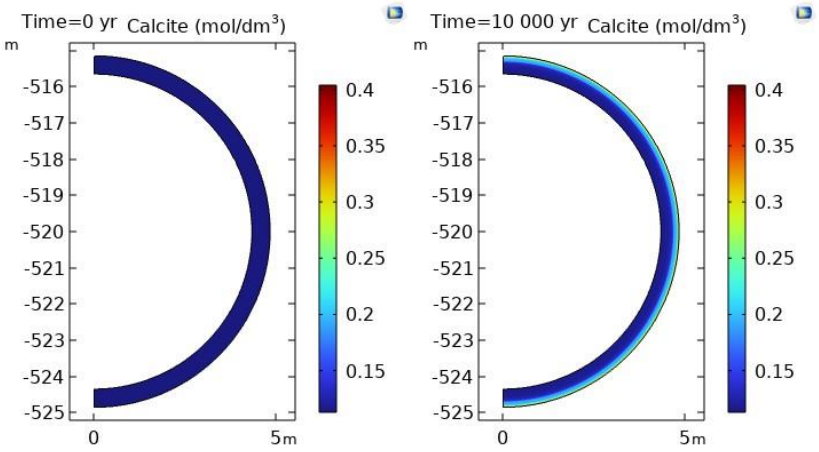

Figure 2.17: Calcite concentration in the liner

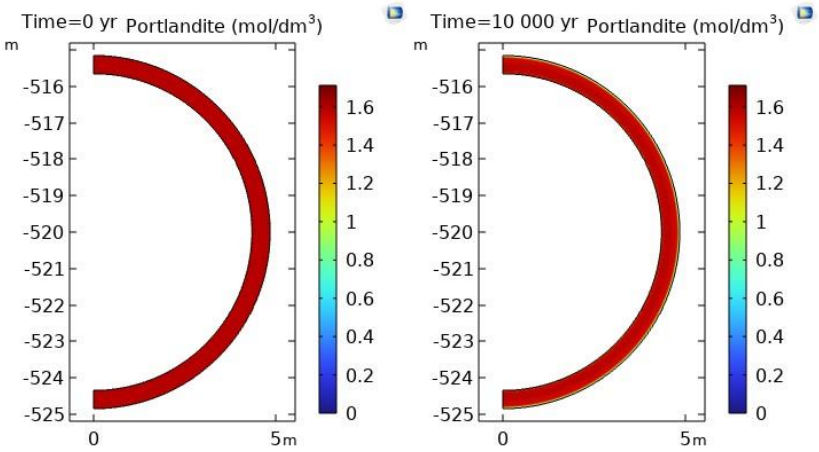

Figure 2.18: Portlandite concentration in the liner

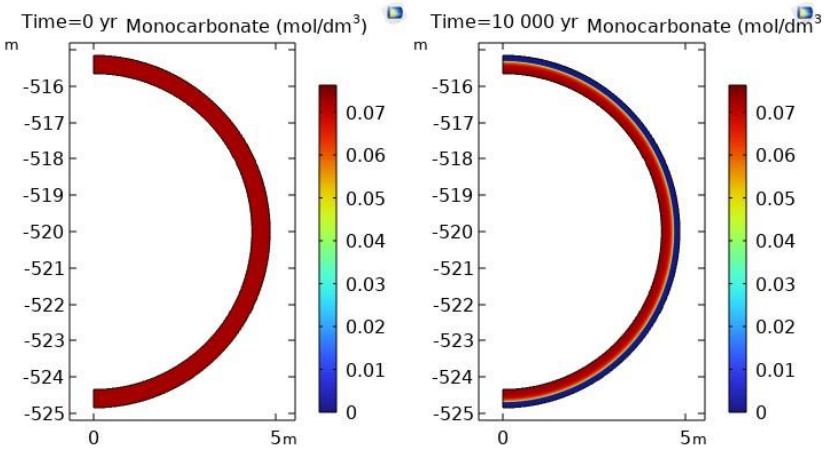

Figure 2.19: Calcium monocarboaluminate concentration in the liner

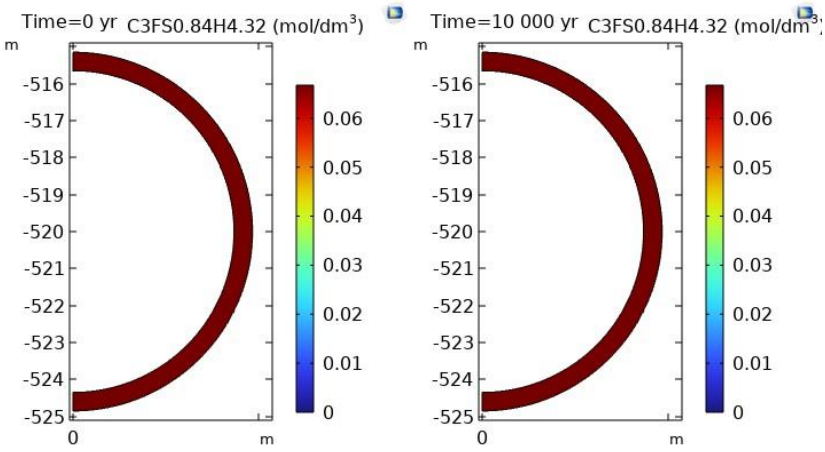

Figure 2.20: $C3FS_{0.84}H_{4.32}$ concentration in the liner

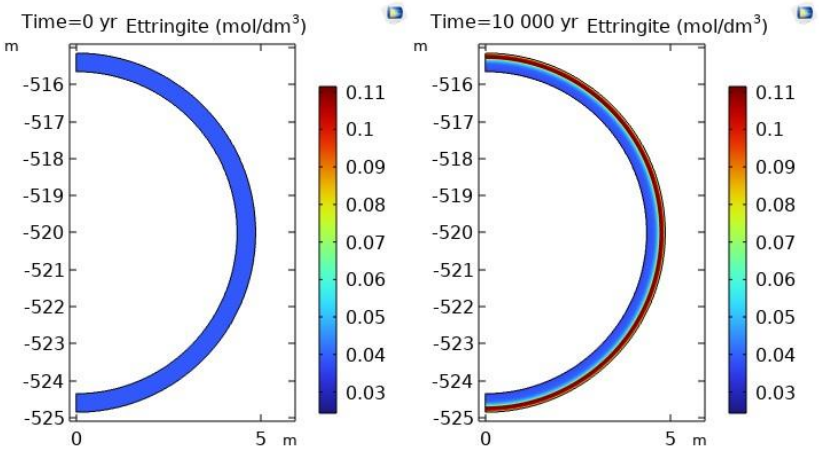

Figure 2.21: Ettringite concentration in the liner

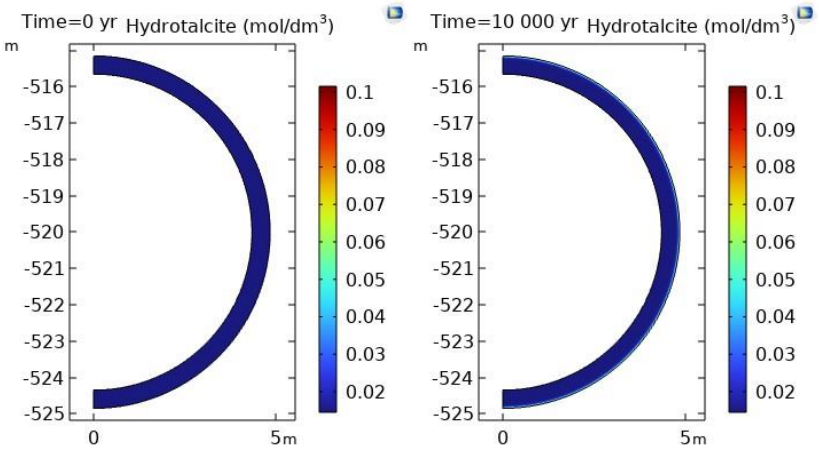

Figure 2.22: Hydrotalcite concentration in the liner

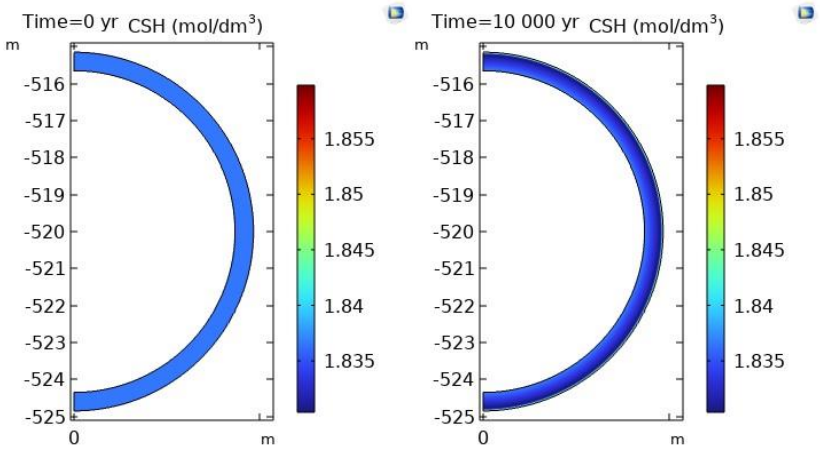

Figure 2.23: CSH concentration in the liner

Based on the modelling results almost no changes occurred for minerals $C3FS_{0.84}H_{4.32}$ and hydrotalcite. Some dissolution of Portlandite and precipitation of calcite took place near the outer liner boundary. More significant changes could be seen for dissolving calcium monocarboaluminate and precipitating ettringite. This could be more clearly seen in Figure 2.24.

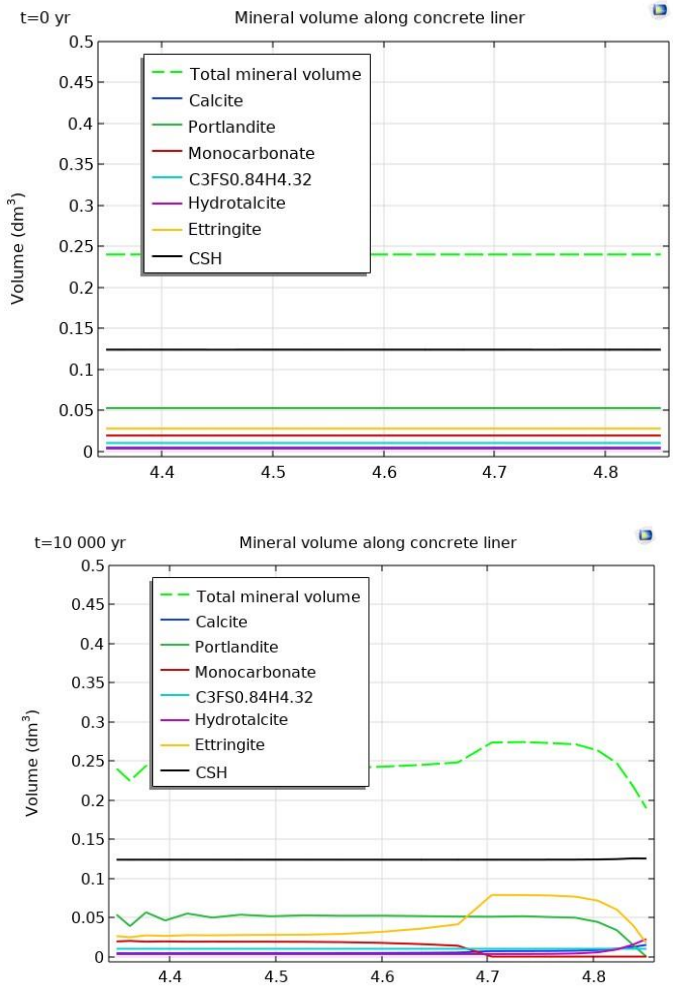

Figure 2.24: Distribution of minerals along concrete liner at different times

The most significant changes in mineral volume (and subsequent changes in porosity) occurred within <20 cm from the outer boundary. The increase of porosity up to a value of 0.16 was observed within ~3 cm from the liner's external boundary, see Figure 2.25.

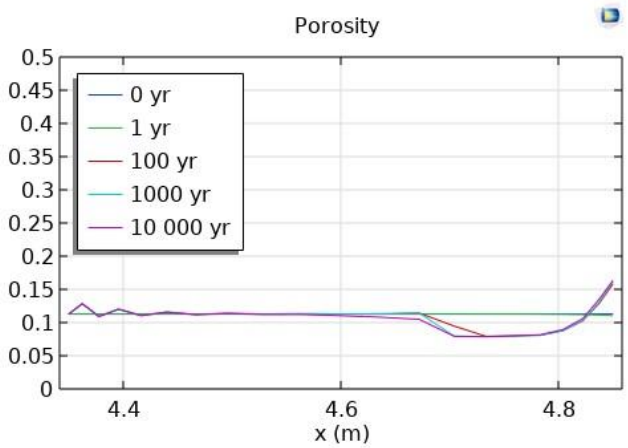

Figure 2.25: Porosity along concrete liner at different times

In case of CSH, some changes could be expected near the outer boundary of the liner. The distribution of the CSH components along the liner is presented in Figure 2.26.

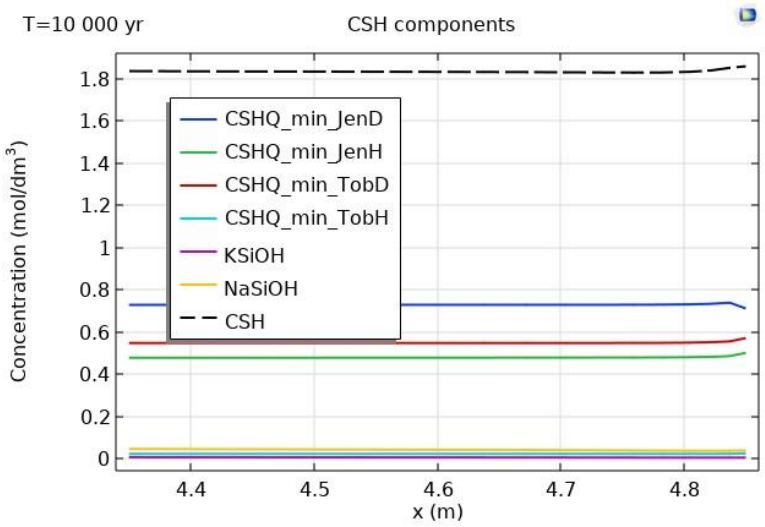

Figure 2.26: Distribution of CSH components

Dissolution/precipitation of different minerals due to transport of various dissolved species from/to concrete and clay host rock led to the porosity change (Figure 2.28). Porosity change subsequently influences solute diffusivity.

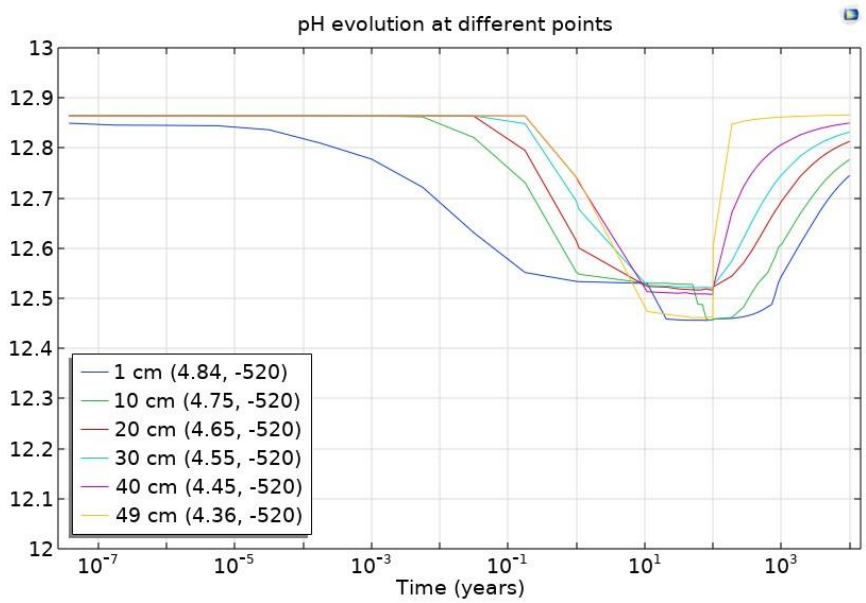

Figure 2.27. pH evolution in points at different distance from concrete liner-rock interface (at 1 cm, 10 cm, 20 cm, 30 cm, 40 cm, 49 cm from liner-rock interface)

Concerning pH, its evolution at different location inside the concrete is given in Figure 2.27 (see Figure 2.12 for the point positions). It can be observed that pH decreases firstly close to the intrados due to the contact with the natural air in the tunnel. It decreases later inside the concrete, but never under 12.4, what preserves the stability of reinforcements.

2.2.3.3 Impact on mechanical characteristics

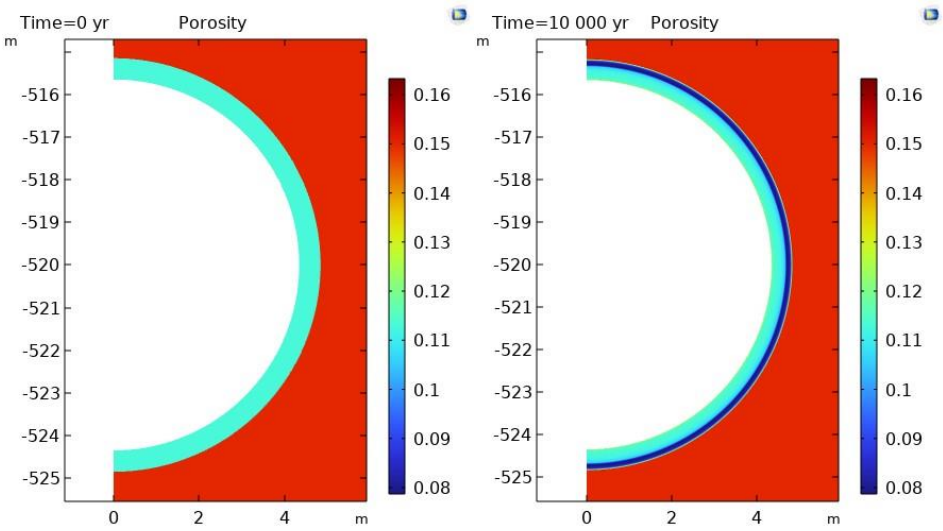

Figure 2.28: Porosity in the concrete liner by the end of simulation

Modelling of chemical interactions of the concrete material with clay host rock porewater allowed to evaluate the change of the concentration of calcium in solid skeleton (Figure 2.29). Considering the concentration of calcium in solid skeleton as an appropriate indicator of mechanical strength of concrete, the change of elasticity modulus could be estimated.

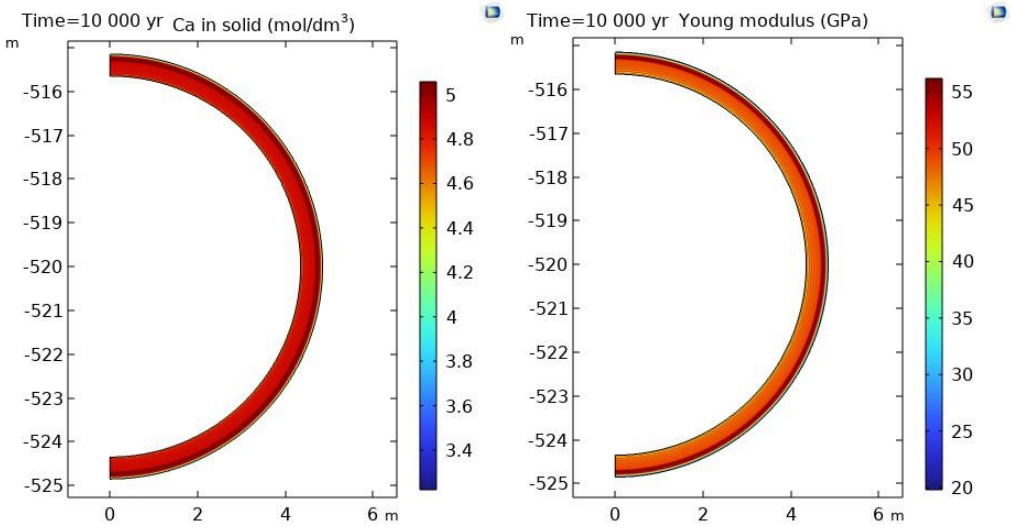

Figure 2.29: The concentration of calcium in solid skeleton and Young modulus

Based on the modelling results, the changes of Young modulus of concrete liner would be expected to a limited extent (<20 cm from the external boundary). Concrete weakening in terms of decreasing elasticity modulus was modelled within ~5 cm of the liner outer part by the end of simulation.

Within subtask 4.3, LEI analysed coupled HMC processes in the safety structure scale. Following the system description in the Base Case, concrete behaviour was analysed under varying conditions imposed by surrounding clay host rock. Direct modelling of reactive transport in line with HM related processes in porous media was performed in two-dimensional geometry. This appeared to be complex and high computational time-consuming task. Due to limited time and computational resources the simulations were run till 10 000 years. For HMC process modelling iCP (interface for COMSOL Multiphysics and Phreeqc sortware) was used. Modelling of coupled HMC processes in predefined system required revision of the mathematical model for unsaturated flow in poroelastic material and definition of coupling terms. Porosity change due to dissolution/precipitation of minerals in concrete material and its impact on solute diffusivity was taken into account dynamically.

2.2.3.4 Summury of LEI contribution

Based on the modelling results under isothermal conditions, it was observed that during the ventilation phase the concrete and surrounding EDZ will become unsaturated. When the EDZ was re-saturated again (after ventilation has finished), the pH value at the concrete-EDZ interface did not returned to the initial pH value of COx porewater (~7). Within certain distance from the liner-EDZ interface the higher pH values were predicted in the EDZ. Within simulation time (10 000 years) no significant pH decrease in the concrete (to 11 and lower) is expected. Thus, it should not impose the chemical degradation of rebars in the concrete and the mechanical strength of the structure. Relating the mechanical properties of concrete (Young modulus) to calcium concentration in solid skeleton, the changes of elasticity modulus would be expected within limited extent (<20 cm) from the liner external boundary. Concrete material weakening in terms of decreasing Young modulus was observed within 5 cm from liner-EDZ interface by the end of simulation (10 000 years). Transport of solutes and potential leaching of calcium from the concrete could be affected not only by porosity change induced by mineral precipitation/dissolution. Impact of mechanical strains on diffusivity and permeability upscaled from smaller scale to safety structure scale are expected to enhance the current model formulation. The developed HMC model could help to predict the design lifetime of concrete structures and transport of radionuclides, considering their sorption and speciation depending on prevailing chemical conditions (pH, redox, etc.)

2.3 Base case interpretation for CSIC

2.3.1 Model description

CODE_BRIGHT [42]has been selected to develop the model and analyse the behaviour of materials. The model has allowed us to numerically observe displacements, variation in porosity and stresses.

Four stages were defined for the creation of the HM model. First, an equilibration phase to determine the initial mechanical and hydraulic conditions. A second stage consisted in designing an excavation sequence and determine the alterations caused in the medium during the drilling. Third, a support structure was constructed as the lining of the cavity. Lastly, the fourth stage consisted in evaluating the long-term behaviour of the entire system. Each of the mentioned stages required to calculate a new equilibrium state prior to compute the next one. The time intervals of each stage were: 200 days to reach the initial steady state, i.e., the equilibration stage, 7 days of excavation, 1 day to construct the support structure and 25 years of evaluation period. This HM model is referred as the “base model”.

To test the potential effect of concrete alteration, we changed the mechanical properties of the support structure in direct contact with the rock, at the concrete-rock interface. This alteration affects the 5 cm of concrete that are closer to the rock, in the outer region of the lining. The aim of this model is to observe the effect over the system of a geochemically-weakened material, considering that in the future it is intended to couple the chemical effect to the problem. For disclosure and comparison purposes, this test model is called “altered model”.

The performed simulations are carried out into an elastic, homogeneous and isothermal medium. It is important to mention that in the long-term it is expected that chemical reactions take place and potentially lead to changes in hydraulic properties (i.e., porosity and permeability) and/or geomechanical properties (i.e., stiffness and strength). Due to the contrasting chemical and mineralogical properties of cementitious materials and rocks (in this case for clay formation), interactions will occur at the cement-rock interface because of the chemical gradients [43]. To perform tests on the model, it has been determined the porosity of the defined altered zone of the concrete support structure was increased and the Young’s modulus in this selected area was decreased in the “altered model”.

To simulate the chemical interaction between concrete and rock, a simple one-dimensional model is applied as shown in Figure 2.30. The considered domain for this problem includes a 5-cm length of the concrete lining, from the rock concrete interface into the concrete material. All domain boundaries are considered to have a no-flux condition and the rock porewater concentration is fixed in the right boundary. Main species from concrete are considered that could react and thus are related to the variation on porosity, according to the results observed in different studies [44]

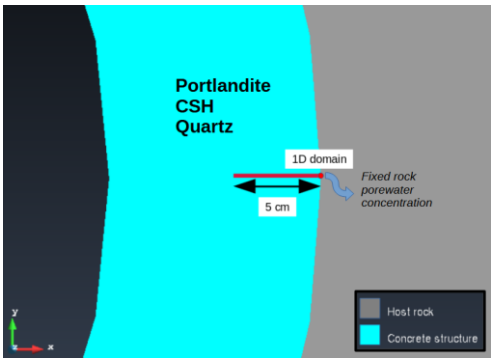

Figure 2.30 : 1D domain for the chemical model

2.3.2 Dimensions

For the HM calculus a two-dimensional modelling has been performed. Figure 2.31 shows a graphical representation of the geometry of the model. The model extends 10 m in the vertical and horizontal directions. The disposal facility is depicted as a circular cavity to simulate a tunnel with a circular cross-

section. Figure 2.31 shows three concentric circles, each of them representing different steps during modelling. The external circle represents the excavation with a 1.30 m radius; the inner circle represents the delimitation of the disposal chamber of 1.00 m in radius. The spacing defined between the external and inner circles areas corresponds to the concrete support structure of a thickness of 0.30-m. There is a circle with a radius of 1.25 m, whose purpose is to show the limit between the concrete with unaltered characteristics and the concrete degraded by chemical reactions. The "base model" consideres the entire 0.30-m thick area as unaltered concrete, while the "altered model" considers a 0.25-m thick area of unaltered concrete and a 0.05-m thick external area of possibly weakened concrete.

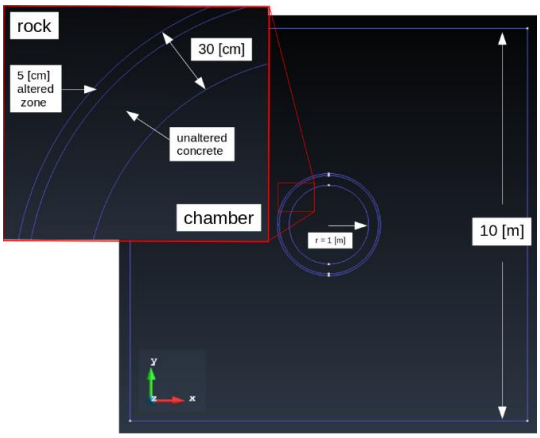

Figure 2.31 : 2D HM model dimensions

The mechanical and hydraulic rock properties were based on measured laboratory results reported by [45] The concrete properties were based on reported data by[46]. For the weakened concrete in the concrete-rock interface of the "altered model", an increased porosity value of 0.25 and 30% decreased Young's modulus were imposed.

It was assumed that the disposal facility was located at 500-m depth. As mechanical boundary conditions, a lithostatic load of 12 MPa was placed on the top boundary of the model. Displacements perpendicular to both vertical and horizontal boundaries were restricted. As flux boundary conditions, a liquid pressure of 5 MPa was applied at the bottom boundary, while no-flux condition were imposed on the remaining borders. The flux boundary condition depended on the stage of modelling. During the steady-state stage, there are no conditions; after the excavation, the system allowed flux at the external 1.30 m radius circle by prescribing atmospheric pressure on it; and after the construction of the concrete support, this condition was set at the inner 1.00-m radius circle.

A structured quadrilateral element type mesh was selected to solve the model. The element size depended on the proximity to the concrete lining. The minimum element size was 0.02 m and constituted the concrete structure and the surrounding rock. The maximum element size was 1 m located at the boundaries. This guaranteed accurate results in the area of interest (concrete-rock interface), and relieved the calculation process, making it more efficient.

2.3.3 Initial and boundary conditions

The initial composition of the concrete is simplified to consider portlandite and calcium-silicate-hydrate (C-S-H) mineral phases as the aggregate. Only changes on the concrete material are evaluated due the setup of the model. Table 10 shows the initial composition selected for each mineral species, where Vol. Fr. is the volume fraction of each mineral phase.

Table 10. Initial composition of concrete for calculations

Material	Mineral	Vol. Fr.
Concrete	CSH	0.091
	Portlandite	0.046
	Porosity	0.15

The composition of concrete for the calculations is based on Lothenbach et al. (2011) [47], adapted for this simplified problem. The Ca/Si ratio of the C-S-H considered in the concrete is 1.6. Potential secondary phases with Ca/Si ratios equal to 0.12 and 0.08 have been considered in the simulations. The Thermodynamic ThermoChimie database [48] version 12a have been selected to provide the required information of mineral phases in Phreeqc simulations.

The initial composition of the rock porewater is assumed to the one given in Table 9, and the initial concrete porewater is based on [47] for fully hydrated cement and equilibrated with the initial cement phases.

Table 11. Initial composition (total molalities) of concrete and rock porewaters. Equilibrium and charge balance constraints are indicated in brackets

Parameter	Concrete	Rock
Na^+	$9.00x10^{-2}$	$2.37x10^{-1}$ (Charge)
K^+	$2.09x10^{-1}$	$1.43x10^{-3}$
Ca^{2+}	$2.49x10^{-3}$ (Portlandite)	$1.52x10^{-2}$
Cl^-	$1.00x10^{-8}$	$2.72x10^{-1}$
$SiO_2(aq)$	$5.87x10^{-5}$ (CSH)	$1.32x10^{-4}$
HCO_3^-	$8.28x10^{-5}$ (Calcite)	$1.47x10^{-3}$ (Calcite)
T (ºC)	25	25
pH (-)	13.63 (Charge)	7.50

The composition of concrete porewater is consistent with the mineral species that constitute this material. This condition guarantees that the porewater in the material does not react with the medium and that the chemical reactions that take place occur near the concrete-rock interface, due to the different composition between both initial porewaters.

2.3.4 Results

Figure 2.32 presents the calculated volume fractions of the different mineral phases interacting as a function of the distance to the interface at different evaluation periods. In the material complete dissolution of portlandite near the interface is observed, together with dissolution of primary C-S-H (Ca/Si ratio = 1.6). During the simulated initial year, only portlandite is observed to dissolve, but by the fifth year, it is observed that primary C-S-H partially dissolves as well. This C-S-H dissolution triggers the precipitation of a secondary C-S-H mineral phase (Ca/Si ratio = 1.2), where the extent of primary phase dissolution correlates with the subsequent precipitation of the secondary phase.

As the years of simulation progress, the dissolution of portlandite extends further into the material. However, the dissolution and precipitation dynamics of the two different C-S-H phases appear to less influence the materia.l.

Figure 2.33 illustrates the computed evolution of porosity near the concrete-rock interface at different intervals during the simulation. The increase in porosity in the material is mainly attributed to the dissolution of portlandite and the dissolution of primary C-S-H (Ca/Si ratio = 1.6). The area of dissolution of portlandite extends over the time, reaching 2.8 cm into the material. The maximum observed value reaches an increased porosity of 0.196.

The dissolution of C-S-H not only leads to an increase in porosity, but also to the precipitation of a secondary C-S-H mineral phase (Ca/Si ratio = 1.2). As primary C-S-H dissolves, the affected area expands up to 0.7 cm from the interface, with a maximum increase in porosity up to 0.23. These results align qualitatively with the observations documented by Soler (2022), who similarly reported increases in porosity in the concrete material as a result of his simulations developed in CrunchFlow.

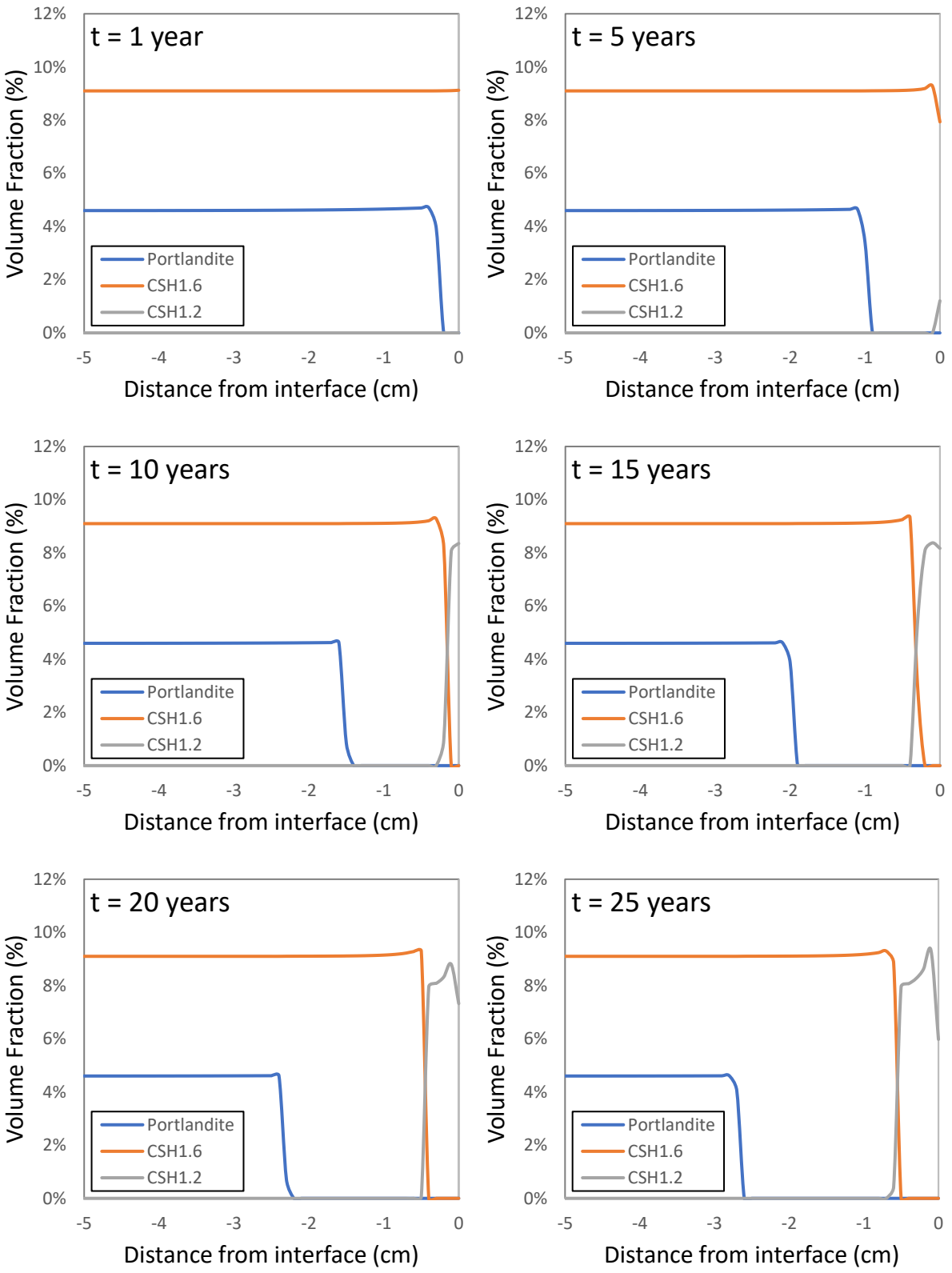

Figure 2.32: Calculated volume fractions in the concrete *vs* distance from the host rock interface at different evaluation periods

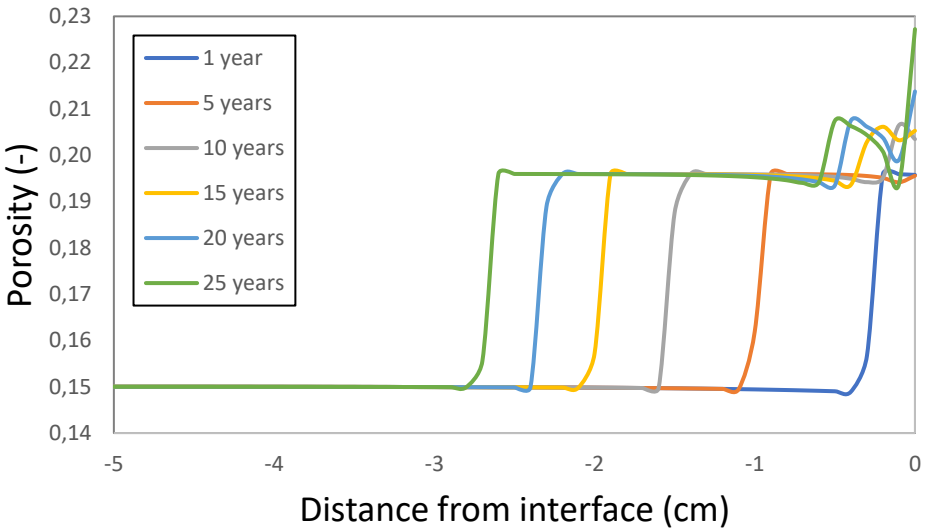

Figure 2.33: Calculated evolution of porosity in the concrete from the concrete-rock interface

Figure 2.34 shows the calculated evolution of pH. There is a pronounced pH gradient between the concrete and the boundary condition representing the rock porewater solution input. As time progresses, the boundary condition increasingly influences the material, gradually affecting the material more extensively.

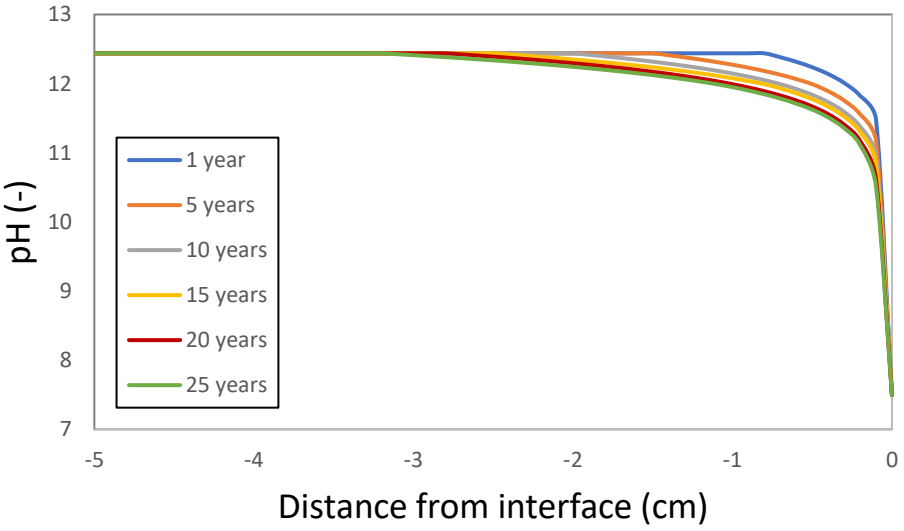

Figure 2.34: Calculated evolution of pH in the concrete model domain

The progression of the chemical system revealed significant portlandite dissolution and considerable chemical evolution of calcium silicate hydrate C-S-H. Dissolution of the primary mineral phase occurred alongside the precipitation of a secondary phase, prevailing the dissolution of minerals over precipitation.

After a 25-year evaluation, a generalized increase in porosity within the concrete structure was predicted. A maximum porosity increase value of 0.23 was reached at the concrete-rock interface, while a value of 0.196 was observed at the maximum affection distance of 2.7 cm from de interface.

Concerning the HM results, a value of 2 mm displacements was observed in the vertical y-axis direction within the support structure. In the horizontal x-axis direction, the displacements observed have a magnitude of 0.8 mm. Similar values were observed in both “base” and “altered” models. In relation with

the variation of porosity of the concrete structure due to the hydro-mechanical effect, it was observed that this parameter remained invariable during the evaluated period of 25 years.

With the calculated liquid pressure and the stresses result data, the mean effective stress and the deviatoric stress have been calculated to plot the stress path of each analysed point and compare differences between “base” and “altered” models. Figure 2.35 presents the stress paths within the concrete support structure.

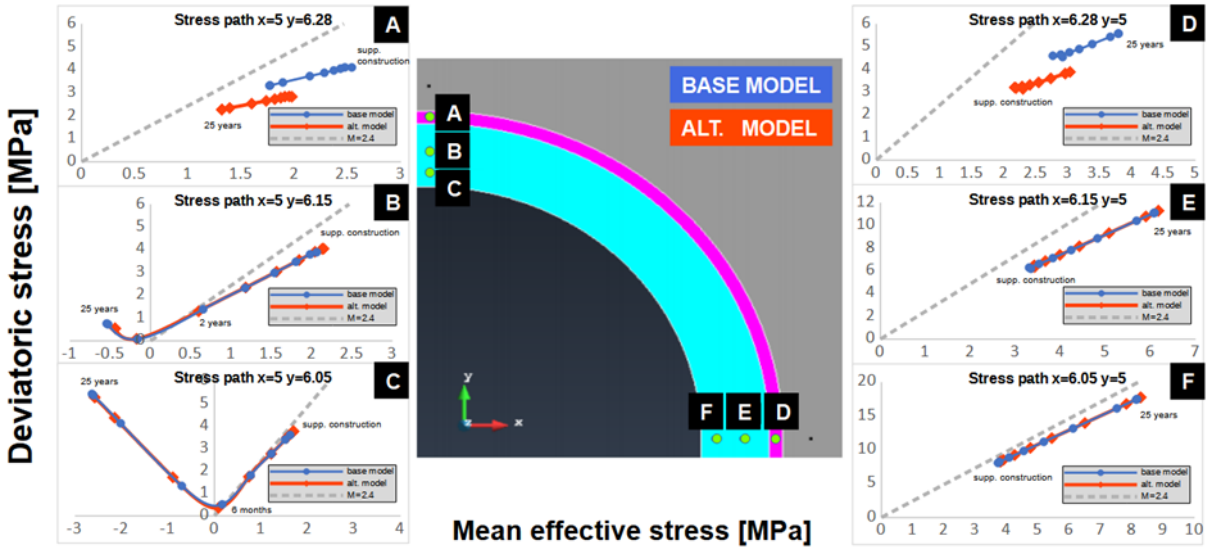

Figure 2.35: Stress path of concrete in the analysed points

In the vertical y-direction within the concrete structure, it was observed that the state of stress was under compression during the 25-year period of simulation and the stress path at point A is below the failure limit in both “base” and “altered” models (Figure 2.35). As long as it is analysed closer to the inner area of the lining, the failure limit was exceeded and the stress state changed. Point B reached failure after 2 years, while point C reaches it after 6 months. On the horizontal x-direction, all support structure points were in a compression stress state and remained below the failure limit during the whole evaluated period. The stress paths observed in points A and D revealed that an altered zone may affect the concrete integrity as a result of lower stress values for a softer material.

3. Conclusion

In this report, the three contributors provided methods and results on their structural modeling. The three strategies of modeling described in this report are capable of considering calcium leaching, cement hydrates neutralization and atmospheric carbonation of concrete. They are all able to consider a realistic variety of hydrates in concrete, and to manage their evolution in the context of leaching coupled with carbonation.

The LMDC model is based on a “reduction of the reactive transport model”,leading to a surrogate chemical model which makes it possible to increase the calculation speed and therefore to address large structural dimensions and long term simulations. They used only three mass balance equations (calcium, carbon dioxide and water). The coupling with the mechanics is based on a homogenization method able to consider the different types of hydrates computed by the chemical surrogate model. These elastic properties are then used to deduce nonlinear properties, especially the creep potential of concrete. The chemical module is then completed by the balance of thermal energy, and the balance of motion; the host rock was also reduced to its effects on the concrete line. This strategy allowed to consider a chemo-mechanical coupling based on micro-mechanics homogenization, and to take into account the creep of chemically degraded concrete. This strategy allowed them to compute the tunnel behavior over one million years. The CSIC and LEI models, on the other hand, retains a complete description of the chemistry of concrete.CSIC provided a detailed description of the chemical interaction between concrete and host rock, but due to their heavy computational cost, the calculus was limited to a small area of a few centimeters around the interface between the two materials, and the time simulated reached only 25 years.

LEI tested a compromise between CSIC and LMDC, using a relatively complete chemical description of concrete in interaction with a meshed host rock, and a linear poro-mechanical model of the soil-structure interaction based on poro elastic properties depending empirically on the chemical state through the calcium concentration in solution. As expected, the LEI model reached an intermediate time of aging of the tunnel (10 000 years). The three strategies of chemical modeling include transport properties depending on the evolution of the porosity. Porosity changes due to concrete mineral dissolution/precipitation were taken into account by solute transport parameters.

The conclusion of this work performed in task 4.3 of Eurad Magic research project, is that different strategies of modeling are possible at structural scale. Among these strategies, three of them have been tested, a first one consisting to couple a classical reactive transports model with a mechanical software thanks to a third software allowing the data and results exchanges between them until the convergence of the both solutions to a coupled one. This strategy, developed by the CSIC, preserves the great ability of each software to model accurately the underlying chemical and mechanical phenomena, but leads to a heavy computational cost limiting both the size of the geometry and the aging to investigate (only a few centimeters during 25 years for the CSIC modeling). The computational cost of the model also leads CSIC to adapt the prescribed conditions of the base case to closer conditions alredy studied by their teams, in order to gain time during parametrization of their model. The second strategy consists to retain the main chemical phenomena, to simplify the mechanicals ones to their linear aspects. This strategy allowed LEI to consider the full 2D geometry (concrete and host rock), and to reach an aging of 10 000 years. The limitation of this strategy is also the computational cost which limits the duration of simulated aging and the realism of the mechanical behavior of the tunnel. The third strategy adopted by LMDC consists to couple all the equations in a single software, but with some simplifications in terms of chemistry. Specifically, for this base case study, the simplifications consist to limit the number of mass balance equations to reduce the computational coast of the chemistry, in order to increase the realism of the mechanical part. This last strategy allowed to use more realistic models for the mechanical part: micro mechanics and homogenization concepts together with nonlinear mechanical behavior of degraded concrete were used, but with a partial representation of the geometry. This last strategy was able to reach the objective of one million years of prediction of the behavior of the tunnel, with a nonlinear mechanical model, but not yet with a full mesh of the host rock. The main conclusion is that, currently, the realism of the chemical modules is acceptable for the three strategies, but the computational

resources being limited, a compromise between the realism of the chemistry and the realism of the mechanical behavior must be done to perform simulation at very long terms.

References

[1] B. Gerard, G. Pijaudier-Cabot, et C. Laborderie, « Coupled diffusion-damage modelling and the implications on failure due to strain localisation », *International Journal of Solids and Structures*, vol. 35, nº 31-32, p. 4107-4120, nov. 1998, doi: 10.1016/S0020-7683(97)00304-1.

[2] R. Mensi, « Séchage du béton: analyse et modélisation », *Materials and Structures*, 1988.

[3] B. Lothenbach, « Thermodynamic equilibrium calculations in cementitious systems », *Mater Struct*, vol. 43, nº 10, p. 1413-1433, déc. 2010, doi: 10.1617/s11527-010-9592-x.

[4] A. Sellier, L. Buffo-Lacarrière, M. E. Gonnouni, et X. Bourbon, « Behavior of HPC nuclear waste disposal structures in leaching environment », *Nuclear Engineering and Design*, vol. 241, nº 1, p. 402-414, janv. 2011, doi: 10.1016/j.nucengdes.2010.11.002.

[5] B. Bary et A. Sellier, « Coupled moisture—carbon dioxide–calcium transfer model for carbonation of concrete », *Cement and Concrete Research*, vol. 34, nº 10, p. 1859-1872, oct. 2004, doi: 10.1016/j.cemconres.2004.01.025.

[6] M. Thiery, « Modelling of atmospheric carbonation of cement based materials considering the kinetic effects and modifications of the microstructure and the hydric state », *Engineering Sciences [physics]. Ecole des Ponts ParisTech, 2005. Phd thesis in frensh. ffpastel-00001517.*, p. 348, 2005.

[7] R. J. Millington, « Gas Diffusion in Porous Media | Science ». Consulté le: 19 juin 2023. [En ligne]. Disponible sur: https://www.science.org/doi/abs/10.1126/science.130.3367.100.b

[8] T. Ishida et K. Maekawa, « MODELING OF PH PROFILE IN PORE WATER BASED ON MASS TRANSPORT AND CHEMICAL EQUILIBRIUM THEORY », *Doboku Gakkai Ronbunshu*, vol. 2000, nº 648, p. 203-215, mai 2000, doi: 10.2208/jscej.2000.648_203.

[9] H. Peycelon, C. Blanc, et C. Mazoin, « Long-term behaviour of concrete Influence of temperature and cement binders on the degradation (decalcification/hydrolysis) in saturated conditions », *Revue européenne de génie civil*, vol. 10, nº 9, p. 1107-1125, nov. 2006, doi: 10.3166/regc.10.1107-1125.

[10] C. Gaël, T. Philippe, A.-M. Abdelkarim, A. Riccardo, et R. Patrick, « Influence de la température sur deux étapes limitantes de la carbonatation : diffusion gazeuse et réactions en solution », vol. 41, 2023.

[11] P. Liu, Z. Yu, et Y. Chen, « Carbonation depth model and carbonated acceleration rate of concrete under different environment », *Cement and Concrete Composites*, vol. 114, p. 103736, nov. 2020, doi: 10.1016/j.cemconcomp.2020.103736.

[12] H.-W. Song, S.-J. Kwon, K.-J. Byun, et C.-K. Park, « Predicting carbonation in early-aged cracked concrete », *Cement and Concrete Research*, vol. 36, nº 5, p. 979-989, mai 2006, doi: 10.1016/j.cemconres.2005.12.019.

[13] L. Granger, « Comportement différé du béton dans les enceintes de centrales nucléaires: analyse et modélisation », *Ecole Nationale des Ponts et Chaussées*, 1995.

[14] L. Buffo-Lacarrière, A. Sellier, G. Escadeillas, et A. Turatsinze, « Multiphasic finite element modeling of concrete hydration », *Cement and Concrete Research*, vol. 37, nº 2, p. 131-138, 2007, doi: 10.1016/j.cemconres.2006.11.010.

[15] N. Hyvert, « Dependency of C–S–H carbonation rate on CO2 pressure to explain transition from accelerated tests to natural carbonation », *Cem. Concr. Res.*, p. 8, 2010.

[16] N. Hyvert, « Application de l'approche probabiliste à la durabilité des produits préfabriqués en béton », These de doctorat, Toulouse 3, 2009. Consulté le: 19 août 2022. [En ligne]. Disponible sur: http://www.theses.fr/2009TOU30030

[17] T. Mori et K. Tanaka, « Average stress in matrix and average elastic energy of materials with misfitting inclusions », *Acta Metallurgica*, vol. 21, nº 5, p. 571-574, mai 1973, doi: 10.1016/0001-6160(73)90064-3.

[18] F.-J. Ulm, F. H. Heukamp, et J. T. Germaine, « Residual design strength of cement-based materials for nuclear waste storage systems », *Nuclear Engineering and Design*, vol. 211, nº 1, p. 51-60, janv. 2002, doi: 10.1016/S0029-5493(01)00430-7.

[19] S. Danèse, « Etude du couplage fissuration-dégradation chimique des bétons : fissure modèle sur pâte de ciment. », *Projet de fin d'études, ENSAIS, Strasbourg, France, 57p.*, 1997.

[20] S. Rahal, A. Sellier, et G. Casaux-Ginestet, « Finite element modelling of permeability in brittle materials cracked in tension », *International Journal of Solids and Structures*, vol. 113-114, p. 85-99, mai 2017, doi: 10.1016/j.ijsolstr.2016.12.023.

[21] A. Sellier, « Anisotropic Damage and Visco-Elasto-Plasticity Applied to Multiphasic Materials ». 2011.

[22] A. Nardi, A. Idiart, P. Trinchero, L. M. De Vries, et J. Molinero, « Interface COMSOL-PHREEQC (iCP), an efficient numerical framework for the solution of coupled multiphysics and geochemistry », *Computers & Geosciences*, vol. 69, p. 10-21, août 2014, doi: 10.1016/j.cageo.2014.04.011.
[23] B. Lothenbach *et al.*, « Cemdata18: A chemical thermodynamic database for hydrated Portland cements and alkali-activated materials », *Cement and Concrete Research*, vol. 115, p. 472-506, janv. 2019, doi: 10.1016/j.cemconres.2018.04.018.
[24] D. A. Kulik, « Improving the structural consistency of C-S-H solid solution thermodynamic models », *Cement and Concrete Research*, vol. 41, nº 5, p. 477-495, mai 2011, doi: 10.1016/j.cemconres.2011.01.012.
[25] L. Ibrahim, L. Lacarrière, et A. Sellier, « EURAD Report of Base case definition. Dissemination level: XX. 06/12/2023. », 2023.
[26] B. Lothenbach, T. Matschei, G. Möschner, et F. P. Glasser, « Thermodynamic modelling of the effect of temperature on the hydration and porosity of Portland cement », *Cement and Concrete Research*, vol. 38, nº 1, p. 1-18, janv. 2008, doi: 10.1016/j.cemconres.2007.08.017.
[27] B. Z. Dilnesa, B. Lothenbach, G. Renaudin, A. Wichser, et D. Kulik, « Synthesis and characterization of hydrogarnet Ca3(AlxFe1 − x)2(SiO4)y(OH)4(3 − y) », *Cement and Concrete Research*, vol. 59, p. 96-111, mai 2014, doi: 10.1016/j.cemconres.2014.02.001.
[28] A. C. Lasaga, *Kinetic theory in the earth sciences*. in Princeton series in geochemistry. Princeton, N.J: Princeton University Press, 1998.
[29] D. L. Parkhurst, K. L. Kipp, et S. R. Charlton, « PHAST Version 2—A program for simulating groundwater flow, solute transport, and multicomponent geochemical reactions: U.S. Geological Survey Techniques and Methods 6–A35, 235 p », Techniques and Methods, 2010.
[30] D. Hu, H. Zhou, F. Zhang, et J. Shao, « Modeling of Short- and Long-Term Chemomechanical Coupling Behavior of Cement-Based Materials », *J. Eng. Mech.*, vol. 140, nº 1, p. 206-218, janv. 2014, doi: 10.1061/(ASCE)EM.1943-7889.0000639.
[31] S. A. Bea, J. Carrera, C. Ayora, F. Batlle, et M. W. Saaltink, « CHEPROO: A Fortran 90 object-oriented module to solve chemical processes in Earth Science models », *Computers & Geosciences*, vol. 35, nº 6, p. 1098-1112, juin 2009, doi: 10.1016/j.cageo.2008.08.010.
[32] D. Rouson, J. Xia, et X. Xu, *Scientific Software Design: The Object-Oriented Way*, 1re éd. Cambridge University Press, 2011. doi: 10.1017/CBO9780511977381.
[33] F. De Gaspari, M. W. Saaltink, J. Carrera, et L. J. Slooten, « Use of redundant data to reduce estimation errors in geochemical speciation », *Applied Geochemistry*, vol. 55, p. 184-191, avr. 2015, doi: 10.1016/j.apgeochem.2014.12.005.
[34] P. Gamazo, L. J. Slooten, J. Carrera, M. W. Saaltink, S. Bea, et J. Soler, « PROOST: object-oriented approach to multiphase reactive transport modeling in porous media », *Journal of Hydroinformatics*, vol. 18, nº 2, p. 310-328, mars 2016, doi: 10.2166/hydro.2015.126.
[35] J. Wang, J. Carrera, M. W. Saaltink, et C. Valhondo, « A general and efficient numerical solution of reactive transport with multirate mass transfer », *Computers & Geosciences*, vol. 158, p. 104953, janv. 2022, doi: 10.1016/j.cageo.2021.104953.
[36] P. Debye et E. Hückel, « The Theory of Electrolytes I. Lowering of Freezing Point and Related Phenomena. Physikalische Zeitschrift, 24, 185-206. », 1923.
[37] J. M. Soler, « CI/CI-D Experiment: 3D Modeling for HTO and 36Cl. Reactive transport modeling of clay-concrete interaction. », 2022.
[38] A. Rima, L. Lacarrière, A. Sellier, P. Chhun, et M.-N. Vu, « Model of water transfer in concrete and rock based on a single state variable to consider simultaneous positive pressure and drying boundary conditions », *Nuclear Engineering and Design*, vol. 413, p. 112499, nov. 2023, doi: 10.1016/j.nucengdes.2023.112499.
[39] E. Neft, « Datasheet COVRA_s concrete. Subject data set for modelling concrete. EURAD MAGIC – February 2023. »
[40] P. Wang, R. Mo, X. Zhou, J. Xu, Z. Jin, et T. Zhao, « A chemo-thermo-damage-transport model for concrete subjected to combined chloride-sulfate attack considering the effect of calcium leaching », *Construction and Building Materials*, vol. 306, p. 124918, nov. 2021, doi: 10.1016/j.conbuildmat.2021.124918.
[41] X. Liu, D. Niu, X. Li, Y. Lv, et Q. Fu, « Pore Solution pH for the Corrosion Initiation of Rebars Embedded in Concrete under a Long-Term Natural Carbonation Reaction », *Applied Sciences*, vol. 8, nº 1, p. 128, janv. 2018, doi: 10.3390/app8010128.
[42] S. Olivella, A. Gens, J. Carrera, et E. E. Alonso, « Numerical formulation for a simulator (CODE_BRIGHT) for the coupled analysis of saline media », *Engineering Computations*, vol. 13, nº 7, p. 87-112, 1996, doi: 10.1108/02644409610151575.

[43] G. Deissmann *et al.*, « Experiments and numerical model studies on interfaces. Final version as of deliverable D2.5 of the HORIZON 2020 project EURAD », EC Grant agreement no: 847593, mai 2021.
[44] E. Kangni-Foli, « Carbonation of model cement pastes: The mineralogical origin of microstructural changes and shrinkage », *Cement and Concrete Research*, 2021.
[45] K. Kim, V. Vilarrasa, et R. Y. Makhnenko, « CO2 Injection Effect on Geomechanical and Flow Properties of Calcite-Rich Reservoirs », 2018.
[46] S. Olivella, J. Vaunat, et A. Rofriguez-Dono, « CODE_BRIGHT 2021 Tutorial Manual. VIII. Tutorial example: Sequential Excavation Method - SEM », 2021.
[47] B. Lothenbach, « CI Experiment: Hydration experiments of OPC, LAC AND ESDRED cements: 1 h to 3.5 years. T. N. Mont Terri Project, 2010-75. », 2011.
[48] J. Rodríguez, D. Pérez, et E. Colàs, « Thecnical report: ThermoChimie version 12a Bibliography. Amphos 21. ThermoChimie project Technical Note TCIII-2023-11E_vs1. », 2023.